THE INFLUENCE OF SNOW COVER ON WINTERTIME NOR'EASTERS

by

Laura E. McGowan

A thesis submitted to the Faculty of the University of Delaware in partial fulfillment of the requirements for the degree of Master of Science in Geography

Spring 2013

THE INFLUENCE OF SNOW COVER

ON WINTERTIME NOR'EASTERS

by

Laura E. McGowan

Approved: _____
Brian Hanson, Ph.D.
Professor in charge of thesis on behalf of the Advisory Committee

Approved: _____
Tracy DeLiberty, Ph.D.
Chair of the Department of Geography

Approved: _____
Nancy M. Targett, Ph.D.
Dean of the College of Earth, Ocean, and Environment

Approved: _____
James G. Richards, Ph.D.
Vice Provost for Graduate and Professional Education

ACKNOWLEDGMENTS

The work presented here would not have been possible without the aid and support of many others.

My deepest gratitude goes out to my entire committee for their patience as I completed my thesis at a distance. In particular, I would like to thank my advisor Brian Hanson for his support, guidance, and positive encouragement over the past few years. His advice and knowledge on running model simulation has been critical to the completion of this thesis and it was his courses in computer programming and climate dynamics that have set the foundation to all my computing research thus far. If it were not for Dan Leathers this project idea would not have been conceived. His direction, advice, and knowledge on nor'easters and snow cover were essential to the work. I am grateful to Dana Veron for her willingness to join my committee on short notice, her rapid feedback, and suggestions to the work.

I would like to thank Kenji Matsuura for his expertise and help computing in the first two years of this project and Gina Henderson for her senior advice and guidance. I appreciate the approachability, friendliness and responsiveness to questions from Ingrid Callaghan, Colleen Leithren, and Linda Brannen over the past few years in the main office. Furthermore, I would like to thank all the teachers I have had in the department during my time at the University which include and are not limited to Tracy DeLiberty, David Legates, Del Levia, Peter Rees, and Edmunds Bunkse. I am truly grateful to have had the opportunity to work in such a friendly

department, with great faculty, and useful computing resources for both my undergraduate and master's work.

Finally I would like to thank my family. They have given me words of encouragement and moral support through the entire process. Without them I would not be where I am today.

TABLE OF CONTENTS

LIST OF TABLES

LIST OF FIGURES

ABSTRACT

The largest alteration that can be made to surface albedo is the addition or removal of snowcover; therefore understanding snow-atmosphere interactions is critical to understanding climatology. The storms of 8-10 February 1969, 25-28 December 1969, 18-20 February 1972, 12-14 March 1993, and 24-26 January 2000 were simulated with the Weather Research and Forecasting Advanced Research Model to examine the impact of snowcover in the continental United States on Nor'easters. Each case was simulated twice. One simulation was initialized with a 50-cm deep snowpack over the Northeast and the other simulation was initialized with the ground void of snow. The model results for the snowpack runs indicate a strong decrease in surface energy budget components leading to a decrease in lower atmospheric temperatures, an increase in pressure, and an increase in stability; however these atmospheric changes did not significantly alter the modeled nor'easters. The nor'easters influenced by the snowpack only had a slight increase in central low pressure and total precipitation and the storm tracks were largely unchanged. The atmospheric modifications from snow are not strong enough to considerably alter the existing upper-level dynamics and geographic controls (cold air damming, land/ocean contrast, etc.) that create and drive cyclones in the Northeast.

Chapter 1

STUDY BACKGROUND

1.1 Introduction

1.1.1 Basic significance of snow

The addition or removal of snow cover is the most significant change that can be made to a landcover in terms of albedo (Kung et al. 1964). The large seasonal cycles of albedo in the middle latitudes are caused by the presence or absence of snow (Kung et al. 1964). Albedo is the ratio of reflected incoming solar radiation to the total incident radiation occurring on a given surface. Albedo affects the amount of available energy at the surface. For example, increasing surface albedo leads to decreased energy absorption by the surface and therefore limits the energy that can heat the near-surface atmosphere (Kung et al. 1964).

Surface albedo forcings are thought to be of the same magnitude as those caused by anthropogenic aerosols, greenhouse gases, and solar variation (Pielke et al. 2002). Snow cover is important to climate studies since a notable shift in snow cover over time could create a major temperature change; therefore understanding the dynamics of snow-atmosphere interactions is essential to understanding all aspects of current and long term climatology (Leathers et al. 1995).

1.1.2 General nor’easter background

A nor'easter is a classic polar front wave cyclone moving along the East Coast of the United States. A surface low develops along the frontal boundary separating an outbreak of cold continental air from warmer maritime air (Kocin and Uccellini 2004). As the low pressure forms and moves northeastward, it brings in warm air from the south via cyclonic circulation. Once the low pressure system hits the Northeast United States the warm air from the south intersects a cold air mass from Canada. The cold air mass is supplied to the Northeast from a high pressure system in Canada spinning anti-cyclonically. They are named nor'easters because during the event residents along the eastern coast of North America are subject strong northeast winds. Each nor’easter affects 35 million people on average (Kocin and Uccellini 2004).

The cyclogenesis of nor'easters is influenced by the topography of the east coast of the United States, including cold air damming behind the Appalachians and the concave coastlines of North Carolina and New England which promote cyclogengesis. Cyclogenesis is also influenced by the thermal land-ocean contrast; cyclones develop quicker over the Atlantic Ocean than in other ocean basins (Kocin and Uccellini 2004).

Snowfall greater than 25 cm typically occurs 100 to 300 km left and parallel to the path of the central low pressure. Little snow falls along the low pressure path because the warming associated with cyclone circulation changes snow to rain (Kocin and Uccellini 2004). Changeovers of rain to snow or ice and vice versa drastically influence snowfall totals, therefore understanding the mechanisms responsible for changes in precipitation type would help to improve forecasts (Kocin and Uccellini 2004).

Knowledge of the interaction between snow and wintertime cyclones in the Northeast will help increase the understanding of the impact of an existing snowpack on nor'easters and further the understanding of the influence of snowcover on the synoptic scale. A greater understanding of these mechanisms could improve nor'easter forecasts. The nor'easters that occurred in February 2010 are a prime example of this. On February 5-6th a nor'easter deposited between 30 to 90 cm of snow from northern Virginia to Southern Pennsylvania and was followed by a second nor'easter 3 days later that added another 10 to 50 cm of snow.

The majority of previous studies on snow-atmosphere interactions focused on local energy fluxes in terms of mesoscale phenomena or teleconnections leaving gaps in the knowledge of snow-atmosphere interactions on the synoptic scale. The research presented here will fill in the knowledge gaps on the synoptic scale which would aid in improving forecasts of nor'easters.

1.2 Physics of the effect of snowcover

1.2.1 Albedo

Winter surface albedo increases quickly from south to north due to latitudinal variations in snow cover. Differences in winter albedo can be as large as 0.67 while differences in maximum summer albedo are around 0.03 (Kung et al. 1964). Snowpack albedo ranges from 0.60 for wet and melting snow to 0.85 for fresh snow. Cloud cover increases snow albedo (Zhang 2005) up to 0.10 (Robinson and Kukla 1985).

Studies comparing maximum and minimum winter snow depths in the mid-latitudes found average differences in albedo of 0.24 with maximum differences up to

0.31 (Cohen and Rind 1991; Kung et al. 1964). Robinson and Kukla (1985) found North American snow covered surface albedo between 35 and 50 °N of 0.56 was approximately three and a half times greater than snow-free surface albedo. In the Great Plains, it was found that a 72 cm forced snowpack increased surface albedo from 0.20 to 0.66 and the increase of 0.46 was spatially consistent (Klingaman et al. 2008).

Snow albedo not only varies with the state of the snow but also with the type of the land cover beneath the snow. For example, the albedo of snow covered farmlands is around 0.60 while the albedo range of forests covered in snow is around 0.35. Different types of trees also have different snowpack albedos; for example, the albedo of pine and hardwood forests centers around 0.28 while aspen and birch forests are around 0.44 (Kung et al. 1964). The lowest snow covered albedos are found in cities when snow is darkened and cleared (Kung et al. 1964).

1.2.2 Energy fluxes

1.2.2.1 Shortwave and longwave

It is expected that snowcover will increase the amount of reflected shortwave radiation. A study analyzing 23 years of observational snow depth data at St. Paul, Minnesota found that outgoing shortwave radiation of a 10 cm or greater snow cover was on average almost four times greater than snow-free conditions. The fourfold increase in shortwave radiation was attributed to the fourfold increase in albedo over the snow covered land (Baker et al. 1992).

Snow not only has a higher albedo but higher emissivity than most other land surfaces. The typical longwave snow emissivity is 0.98 (Zhang 2005). The higher

emissivity of snow means snow is closer to acting like a black body over the infrared spectrum, emitting more outgoing longwave radiation (OLR) and cooling the surface. During cold, dry, cloud-free conditions the higher emissivity of snow cools the surface and creates a low level inversion. Higher emissivity also means higher absorptivity, therefore on cloudy days, when there is an increase in downwelling longwave radiation; the snow cover could potentially absorb more longwave energy, creating higher surface temperatures (Zhang 2005). Under cloudy skies there is increased downwelling longwave radiation which can act to increase surface outgoing longwave radiation; therefore there is a potential for no net longwave radiation change.

Baker et al. (1992) found OLR was second to outgoing shortwave radiation for the largest differences in radiation between snow and snow-free conditions. Although there was increased emissivity for the snow the OLR was approximately 45 W m^{-2} lower in the maximum snow simulation because the snow typically had lower surface temperatures.

While Baker et al. (1992) found OLR decreased for the snow covered land a significant trend was not found in net longwave radiation for snow versus snow-free conditions (Baker et al. 1992). Results from a one-dimensional snowpack model with varied albedo and depth in the Great Plains showed that OLR is always greater than downwelling longwave radiation over a snowpack; therefore the net longwave radiation is always directed away from the surface. Similar to Baker et al. (1992) the study showed that higher albedo snow surfaces have smaller OLR due to cooler surfaces temperatures which results in smaller absolute net longwave radiation values (Ellis and Leathers 1999). The differences in the net longwave radiation among the

different albedo scenarios were only apparent during the day (Ellis and Leathers 1999).

1.2.2.2 Sensible and latent heat

Sensible heat is heat transferred by conduction or convection resulting in a temperature change. When snow covers the land the overlaying atmosphere is typically warmer than the land surface and therefore the sensible heat flux is expected to be directed toward the surface. Calculations from a snowpack model and snowpack data in the U.S. Great Plains, found deeper snowpacks with higher albedos had sensible heat directed toward the surface, removing heat from the atmosphere and cooling the air mass above; while lower snow albedos, typical for melting and discontinuous snow cover, had sensible heat flux directed from the surface to the atmosphere warming the overlying air mass (Ellis and Leathers 1999). At night there was little difference in the sensible heat flux between surfaces with different snow albedos (Ellis and Leathers 1999). A general circulation model study, with a forced snowcover in the Great Plains, found that the sensible heat flux directed from the atmosphere to the surface was over 30 W m^{-2} greater over the snow (Klingaman et al. 2008).

Latent heat is the energy exchanged when water changes phase. Melting snow is a latent heat sink while freezing is a latent heat source. The changes in latent heat due to snowcover are greatest in lower latitudes and in the spring when there is greater insolation. Similar to the sensible heat and longwave radiative surface fluxes there were only small differences in latent heat flux at night among the different albedo scenarios (Ellis and Leathers 1999).

The presence of a snowpack below a wintertime cyclone reduced latent heat flux compared to snow-free scenarios (Elguindi et al. 2005). Ellis and Leathers (1999) found latent heat flux over a snowpack is directed from the surface into the atmosphere regardless of snow albedo; since snow is supplying vapor to the overlying dry air. The absolute magnitude of the latent heat flux into the atmosphere is greater over lower albedo snow. Ellis and Leathers (1999) attributed the increased latent heat flux to the warmer temperatures of the lower albedo snow increasing the accessibility of moisture flux into the atmosphere via sublimation or melting.

1.2.2.3 Net surface energy budget

Both net surface radiation and net surface energy budgets of snow covered surfaces have been reported (Baker et al., 1992; Cohen and Rind, 1991; Ellis and Leathers, 1998; Ellis and Leathers, 1999). Net surface radiation is the sum of the net longwave radiation and net shortwave radiation and the net surface energy budget is defined as the sum of the net surface radiation plus sensible and latent heat flux from the surface, and ground heat flux (the heat flux from the surface into the ground).

Baker et al. (1992) found snowpacks decreased net radiation at the surface. Under snow-free conditions the net radiation was directed toward the surface at 32.28 W m^{-2} while for snow depths greater than 10 cm the net surface energy was 14.16 W m^{-2} and directed toward the atmosphere. The net radiative flux at the surface for snow depth less than 10 cm was 3.36 W m^{-2} and directed toward the surface, indicating that a loss of surface radiative energy to the atmosphere only occurs if the snowcover completely covers the surface.

On monthly scales, Cohen and Rind (1991) observed a decrease in snow covered ground temperature of approximately 0.7°C. Cohen and Rind (1991) expected

to find a decrease in the surface energy budget of the snowpack where the surface losses energy to the overlying atmosphere; however the only term in their net surface energy budget that increased energy loss from the surface was absorbed shortwave radiation. The sensible and latent heat fluxes toward the snow surface were large enough to cancel out the shortwave flux loss, creating a net gain in energy surface energy fluxes directed toward the surface. However when Cohen and Rind (1991) included the snowmelt term in their energy budget calculation the result was a 0.5 W m^{-2} net flux away from the surface, explaining the observed decrease in temperature of the snowpack.

On short time scales, snowcover results in a loss in net surface energy to the atmosphere due to changes in shortwave radiation and ground heat flux. Snow has an albedo higher than almost any other land surface leading to a reduction in the amount of shortwave radiation that is absorbed at the surface, thus increasing the reflected shortwave radiation to the atmosphere. Snow acts as an insulator to the ground and therefore there will be reduced ground heat flux from the soil.

Both latent heat and net longwave flux terms over a snowpack can either act to increase or decrease the net energy budget at the surface. Melting snow results in a loss of latent heat at the surface to the atmosphere and freezing snow results in a gain in latent heat at the surface. OLR depends on both the temperature and emissivity of a surface. The increased emissivity of snow increases OLR from the surface to the atmosphere while decreased surface temperatures of the snowpack can decrease the OLR from the surface.

Sensible heat will typically be directed toward a snowpack since the snow is cooler than the overlaying atmosphere.

1.2.3 Temperature

Decreases in net surface energy budget due to the presence of snowcover reduce surface temperatures. Baker et al. (1992) found daily mean temperatures were 8.5°C cooler for a snowpack greater than 10 cm compared to snow-free conditions. A study of discontinuous snow cover in the Great Plains found air mass temperatures were 1 to 4°C cooler over snow-covered versus snow-free land (Ellis and Leathers 1998). Klingaman et al. (2008) found two-meter air temperatures were 2 to 8°C lower over a snowpack. Simulations of maximum and minimum snow boundaries in North America found the near surface temperature were between 5 and 10°C lower in the maximum snow simulation (Walsh and Ross 1988).

1.2.3.1 Maximum and minimum temperature depressions

The difference between atmospheric temperatures above snow and snow-free surfaces are frequently compared and are referred to as air temperature depressions. Baker et al. (1992) found maximum and minimum air temperatures depressions of 8.5°C. In contrast, Namias (1985) found maximum air temperature depressions will be larger than minimum air temperature depressions because there is no albedo affect at night. Similar to Namias, an observational study of snow-free conditions and snowpack conditions greater than 2.5 cm in the Northeast showed that snowpack decreased maximum air temperatures by approximately 6°C and minimum temperature by about 5°C (Leathers et al. 1995). Ellis and Leathers (1999) found that increasing surface albedo lowered the mean daytime air mass temperature by approximately 5°C and the maximum daily temperature around 8°C, but did not change the nighttime temperature significantly.

Cohen and Rind (1991) used the albedo difference between maximum and minimum snowcover in a one-degree energy budget model to calculate a temperature difference between the maximum and minimum snowcover. The calculated temperature difference was double the observed temperature differences; therefore temperature depressions were not as large as expected from differences in albedo and absorbed shortwave radiation.

1.2.3.2 Temperature profile

Numerical simulations of twenty consecutive Januaries over the entire northern hemisphere for a higher than average snow extent and a lower than normal snow extent found increased snow extent reduced temperature in the bottom 75 m of the atmosphere over the United States and Canada (Walland and Simmond 1996). The temperature reductions were as high as 6°C in areas where the snow cover was extensive in both simulations, such as the Arctic. Temperature reductions extended beyond the lower-levels of the atmosphere. Temperature reductions at 850 mb were similar in extent to near surface temperatures but had a smaller magnitude. Patchy cooling extended to 500 mb in the mid-latitudes and beyond 500 mb in northern Polar Regions (Walland and Simmond 1996).

1.2.3.3 Temporal and spatial distribution of temperature depression

In the Northeast United States, increased temperature depressions have been reported in late and early winter compared to mid-winter (Leathers et al. 1995). The increased depressions are believed to be due to increased solar zenith angle (greater incoming solar radiation means more shortwave radiation is reflected compared to a snow-free surface). Zhang (2005) hypothesized that even if the albedo is lower in the

spring due to melting, the albedo effect on decreasing temperature is actually greater because of the increased radiation. Zhang (2005) also attributes increased zenith angle to a larger snow albedo affect in lower and mid-latitudes.

Leathers et al. (1995) found the maximum temperature depressions were greatest in the Spring and Fall seasons with a range of 7.9°C in late April to 4.6°C in early February. Minimum temperature depressions were more temporally consistent. Minimum temperatures had a slight increase in midwinter which was attributed to the longer nights increasing the radiation effects and more homogenous and deeper snow cover decreasing the flux from the soil (Leathers et al. 1995).

The increase in early and late season maximum temperature depression is attributed to synoptic forcing of cold air masses from central Canada rather than solar zenith angle. The change was attributed to synoptic forcing because it is unlikely to have significant snowfall in early and late seasons without an uncharacteristically cold air mass. In addition, the snowmelt in early and late seasons creates an energy sink into the snow and cools temperatures (Leathers et al. 1995).

Leathers et al. (1995) found that the relationship between snow cover and air temperature in the Northeast are highly dependent on geographic position and typical air mass characteristics and only slightly dependent on seasonality. Larger variations in temperature depression occurred spatially rather than temporally.

Some studies did not find temporal changes in temperature depression. Baker et al. (1992) was unable to find a clear seasonal trend in temperature depressions associated with a snow pack. Cohen and Rind (1991) found that on a weekly time scale the effect of snow cover on temperature is independent of the winter month chosen.

Increased clouds and moisture nearing the coast decrease the radiative effects of snow cover and therefore decrease the maximum and minimum temperature depression (Leathers et al. 1995). Maximum temperature depressions also decrease toward the south, most likely due to air mass characteristics and not latitudinal differences in the absorbed shortwave radiation.

1.2.4 Pressure

Utilizing a GCM to compare snowlines simulated at 50 and 40 °N, it was found that the southward shift of the snowline increased the monsoonal pressure difference between the continent and the ocean in the Northern Hemisphere (Spar 1973). The same study observed a decrease in central low pressure of a cyclonic event of 3 mb for the smaller snow extent attributed to decreased baroclinicity associated with the northerly snowline creating a weaker cyclone (Spar 1973).

Walsh and Ross (1988) found sea level pressure in maximum snow cover simulations in North America decreased up to 5 mb when compared to minimum snow cover simulations. Since an increase in pressure was not seen above 800 mb in the maximum snow cover simulation, the higher pressure was attributed to surface cooling. In addition, the maximum snow cover has slightly lower sea level pressure off the East Coast of the United States (Walsh and Ross 1988).

Elguindi et al. (2005) found the central low pressure of a cyclone in a maximum snowpack simulation increased by an average of 4 mb, and the increase ranged from 0.4 to 10.0 mb. Walland and Simmond (1996) also found average central low pressure increased for maximum snow cover. Elguindi et al. (2005) noted that the differences in central low pressure were not sizeable but of importance because surface energy fluxes are not the primary driving forces of continental wintertime

cyclones. The study also found the strongest storms and late season storms had the largest changes in pressure due to snowcover. Therefore, the study concluded that the main effect of the snow cover was to limit intensification (Elguindi et al. 2005).

1.2.5 Baroclinicity and stability

A comparison of simulations of a higher than average snow extent and a lower than normal snow extent in the Northern Hemisphere found that greater snow extent weakened the pole-to-pole temperature gradient in the North Atlantic by reducing temperatures in lower latitudes and increasing temperatures in higher latitudes (Walland and Simmonds 1996). Cohen and Rind (1991) found maximum snow cover simulations had more stable atmospheric conditions. The increased stability resulted in more sensible heat flux and latent heat flux trapped at the surface.

Walland and Simmond (1996) found the average central low pressure increased for maximum snow cover; therefore the shallower atmosphere weakened storm tracks due to decreased storm density and decreased cyclone speed. The cyclogenesis decreased for maximum snowcover because at 500 mb there was a decrease in meridional (north to south) temperature gradient that therefore decreased baroclinic instability in the lower levels of troposphere and decreased the area for cyclonic development (Walland and Simmond (1996).

1.2.6 Precipitation and clouds

Namias (1985) attributed increased near-surface static stability over the snowpack to the observed decrease in precipitation in the Midwest and Eastern United States. Walland and Simmond (1996) found areas with the greatest changes in precipitation due to snow cover were remote from the snow boundary forcing.

Walland and Simmond (1996) believed this might be due to the fact that precipitation values over the snow cover are typically low, making the magnitude of differences in precipitation smaller.

Cohen and Rind (1991) found the cloud cover and atmospheric albedo decreased by 2 % in the maximum snow cover simulation. In the Great Plains, cloud cover increased over the snow forced area and downwind because the cool dry air over the snowpack acted like a permanent front along the edge of the snowpack. Therefore, when southerly winds were advected over the snowpack to the Northeast, the cold air over the snowpack forced warm moist air to rise and enhance upward motion (Klingaman et al. 2008).

Elguindi et al. (2005) found cyclones over a snowpack experienced the greatest cooling and drying in warm sectors compared to adjacent cool sectors because cooling and drying have less affect where temperature and moisture are already low. The cooled warm sector became similar to adjacent cold and cool sectors and the temperature and moisture gradients between sectors was reduced therefore frontal strength was reduced (i.e., cold and warm fronts). The temperature gradient across the cold front was reduced by approximately 15% in the snowpack simulation, and in some cases the reduced temperature gradients in the lower troposphere reduced positive feedback between the surface and the mid-troposphere, preventing cyclone growth and strengthening (Elguindi et al. 2005). The decreased temperatures and sensible heat flux create increased stability in the warm sector (with an inversion near the surface) decreasing precipitation and cloud cover; latent heat flux and cyclone strength were also reduced since cloud development and precipitation processes are

responsible for latent heat release and thereby cyclone development (Elguindi et al. 2005).

In some cases, the reduced strength of the cold front in the perturbed simulation brought about decreased upward vertical velocity along the fronts that reduced cloud development and precipitation. Weakened fronts can reduce the strength of uplift, cloud development, precipitation, and cyclonic wind-shear; all ultimately diminish cyclone strength. Most cases had a decrease in upward vertical motion near surface in central lower pressure (Elguindi et al. 2005).

1.3 Simulating the response of nor'easters to snowcover

The aforementioned studies have shown many ways in which the atmosphere responds to the presence of snowcover. Some of the changes are direct, for example the cooling and drying of the lower atmosphere; while others are indirect and depend on the atmospheric response to surface flux changes. Given the importance of nor'easters to winter weather in the Northeastern United States, and the fact that small changes in storm track can drastically influence regional weather damage, it is valuable to see if the similar changes in intensity and track that occurred for Midwestern cyclones (Elguindi et al. 2005) occur for nor'easters.

Chapter 2

MODEL SETUP

2.1 Simulation configuration

2.1.1 Study location

The Northeast was chosen as the study location because unique winter time cyclones (nor'easters) occur in a densely populated region. Close to twenty percent of the United States Population lives in this area (U.S. Census Bureau 2010). The Northeast is an ideal study area to examine geographic controls influencing snow-atmosphere exchanges because there are large changes in inter-and-intraannual snow cover and in elevation, and because the region is influenced by both the Atlantic Ocean and the Great Lakes (Leathers et al. 1995). The topography of the Northeast influences nor'easters. The concave coastlines of North Carolina and New England promote cyclogenesis (Kocin and Uccellini 2004) because the thermal contrast of land and ocean creates enhanced baroclinicity, the Atlantic Ocean supplies latent heat and warm waters in the winter which can enhance cyclogenesis, and the Appalachians act to dam cold air from the North along the coast.

2.1.2 Domain and time scale

A two-way triple nested domain was utilized in the simulations. In two-way nesting the parent grid feeds information into the nested grid which ultimately feeds information back to the parent grid. Domain gridding decreased with a three-to-one

ratio from the parent to the nested domain. The outer domain grid-cell size was 135 by 135 km, the second domain was 45 by 45 km, and the inner domain was 15 by 15 km (Figure 2.1.1).

Each simulation was run for 108 hours (4.5 days). The simulations were each initialized 24 hours before the storm reached the United States East Coast allowing for model “spin-up”.

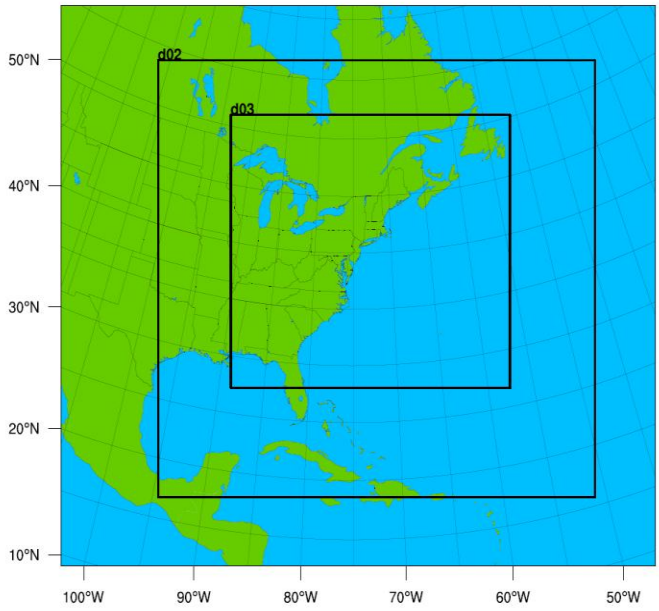

Figure 2.1.1: The triple nested domains utilized in the WRF-ARW simulations with grid spacing of 135, 45 and 15 km respectively for the nested domains three, two, and one.

2.1.3 Snowpack

The perturbed simulation was initialized with a snowpack extending from the southern portions of Virginia north into Canada and from eastern Indiana west to the Atlantic (Figure 2.1.1). All three domains in the control simulation were void of snow cover for model initialization.

The snowpack is initialized with a snow depth of 50 cm to decrease or eliminate heat flux from the soil and ensure that during the four and half day simulations the bulk of the snowpack in the perturbed run remained homogenous and intact even with significant melting. Increasing snow depth increases snow albedo until approximately 15 cm depth. After 15 cm, changes in snow albedo are due solely to change in crystal structure (i.e., age and condition of the snow) (Kung et al. 1964; Robinson and Kukla 1985). Since albedo changes due to crystal structure transformations are small, the snow albedo generally plateaus at depths greater than 15 cm.

With 50 cm of snow, a significant amount melt or ablation would need to be removed to expose groundcover. A 50 cm snow depth extending to southern Virginia is idealized and was done to emphasize and intensify the effect of the snowpack on the atmosphere that might have been unclear with a weaker forcing (i.e., allows for the isolation of the influence of the snowpack). The snow is not added back if it is melted or evaporated to prevent creating an infinite latent heat sink; furthermore snow is allowed to accumulate in both the perturbed and control simulations.

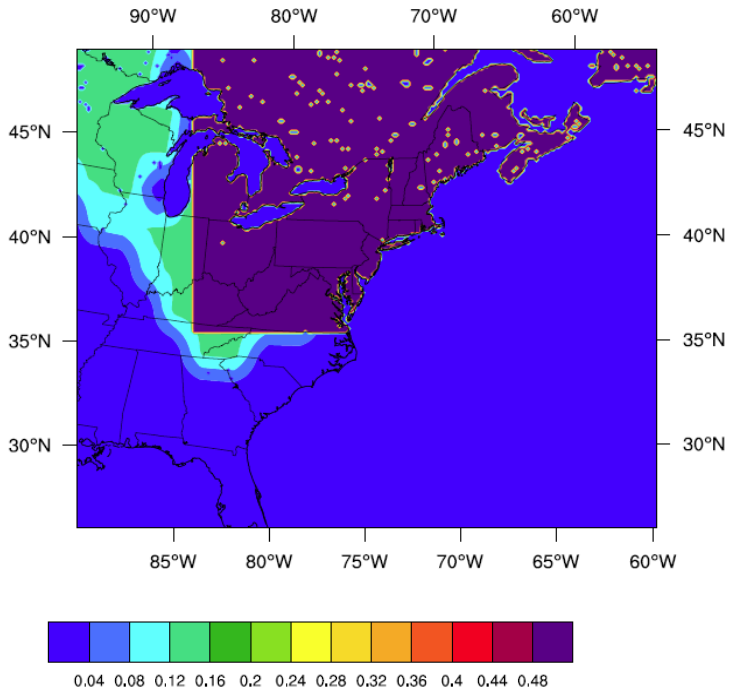

Figure 2.1.2: The snow extent in the inner most domain for perturbed simulations.

2.1.4 Case Selection

Study cases were selected from the thirty-two snow storms presented in Northeast Snowstorms Volume II: The Cases (Kocin and Uccelini 2004b). The number of cases used in this study were constrained by computational resources. To narrow the number of cases and make the cases more homogenous, only classic nor'easters as defined by Kocin and Uccelini (2004) were investigated. Classic nor’easters have a classic polar frontal wave where the surface low develops along the frontal boundary separating an outbreak of cold continental air from warmer maritime air over or near the Gulf of Mexico and a secondary low pressure does not develop.

The March 1993 case is considered one of the best examples (Kocin and Uccellini 2004). Non-classic nor'easters have a secondary low pressure develop. Sixteen out of thirty-two cases were considered classic nor'easters. To further reduce the number of cases, classic nor'easters that experienced a center jump were eliminated, leaving six cases.

Although a classic nor'easter without a central low pressure jump was narrow enough criteria to create a set of cases, seasonality was also considered in the case selection process. Cases that spanned several seasons were selected to make sure the simulations were not seasonally biased. The resulting set consisted of one late season (March), one early season (December) and three mid-season storms (one in January and two in February). The simulated cases were the storms of 8-10 February 1969, 25-28 December 1969, 18-20 February 1972, 12-14 March 1993, and, 24-26 January 2000.

2.2 Model background

Nor'easters with varying snowcover conditions were simulated with the Weather Research and Forecasting Advanced Research Model (WRF-ARW) Version 3.1.1, a mesoscale-to-synoptic scale model from the National Center for Atmospheric Research (NCAR). WRF-ARW is an advanced flexible nonhydrostatic model (with hydrostatic options). The model has a variety of interchangeable physics components allowing for real data studies or weather prediction and idealized studies (Skamarock et al. 2008; Wang et al. 2009). The WRF modeling environment was developed by NCAR in conjunction with the National Oceanic and Atmospheric Administration, the Air Force Weather Agency, the Naval Research Laboratory, the University of Oklahoma, and the Federal Aviation Administration (Wang et al. 2009).

The following briefly summarizes the basic dynamics and operation of WRF-ARW. More detail on the model is described in the technical documentation (Skamarock et al. 2008).

2.3 Governing equations

The model utilized nonhydrostatic Eulerian dynamics in a terrain-following vertical coordinate system called η-coordinates. These pressure-ratio coordinates use the atmospheric pressure difference between the top layer of the atmosphere and the surface, μ, as a denominator, and are essentially equivalent to σ-coordinates commonly used (Washington and Parkinson 2005). The equations of motion contain the usual advected time derivative, pressure gradient, and body force terms for an (x,y,η) coordinate system with (u,v,w) velocity components.

$$\partial_t U + (\nabla \cdot Vu) - \partial_x\left(p\partial_\eta \phi\right) + \partial_\eta(p\partial_x \phi) = F_U \qquad 2.2.1$$

$$\partial_t V + (\nabla \cdot Vv) - \partial_Y\left(p\partial_\eta \phi\right) + \partial_\eta(p\partial_Y \phi) = F_V \qquad 2.2.2$$

$$\partial_t W + (\nabla \cdot Vw) - g\left(\partial_\eta p - \mu\right) = F_W \qquad 2.2.3$$

The uppercase forms of the velocity components (*U,V,W*) are the product of μ and their corresponding velocity components, ϕ = *gz* is geopotential, and *p* is pressure. The *F* terms include all of the body forces that arise from thermodynamic forcing, gravity, friction, and rotational effects.

The other prognostic terms are conservation of dry air mass and conservation of thermal energy, both presented as change equals flux plus source equations. The Euler Flux terms for WRF are below (Skamarock et al. 2008).

$$\partial_t \theta + (\mathbf{V} \cdot \nabla \theta) = F_\theta \qquad 2.2.4$$

$$\partial_t \phi + \mu^{-1}[(\mathbf{V} \cdot \nabla \phi) - gW] = 0 \qquad 2.2.5$$

where θ is potential temperature and g is gravitational acceleration.

Equations 2.2.1 through 2.2.5 are implemented for dry air and then duplicated for moisture.

The model operates in a coordinate grid laid over a projected map surface. Within this project, the projection used was lambert conformal. The horizontal derivative operators, ∂ in the above equations, as well as the curvature effects, are defined based on the projection used. For improved numerical stability, the equations are recast into perturbation forms before setting up the discretized solution procedure.

2.4 Model physics

The physics options selected were based on those that were most recommended, the most simulated schemes, the least computationally expensive schemes, and those that gave the appropriate type of output. The following sections describe the selections made. For explicitly resolved precipitation, we utilized WRF single-moment 6-class microphysics scheme (WSM6). Output precipitation types are liquid convective, liquid non-convective, snow, and an ice/graupel combination (Wang et al. 2009). Non-convective precipitation is grid scale and convective precipitation is subgrid scale precipitation calculated from the Kain-Fritsch cumulus parameterizations scheme (Wang et al. 2009).

The Rapid Radiative Transfer Model (RRTM) scheme was selected for longwave radiation. The RRTM scheme includes several bands and trace gases (Wang

et al. 2009). The Dudhia scheme was chosen for shortwave radiation which integrates downward radiative flux and has absorption and scattering for both cloudy and clear skies (Wang et al. 2009).

The Yonsei University scheme was selected for the planetary boundary layer and the MM5 similarity theory was selected as the surface layer scheme.

2.4.1 Land surface model

The NOAH community land-surface model was used. NOAH is an acronym representing the collaborators and developers of the model; NCEP Environmental Modeling Center (NCEP/EMC), Oregon State University (OSU), Air Force Weather Agency (AFWA) and Air Force Research Lab (AFRL), and NWS Hydrology Lab (HRL) (Mitchell et al. 2005). NOAH LSM calculates soil moisture, both soil and skin temperature, snowpack depth and its water equivalent, canopy water content, and both energy and water flux terms (Mitchell et al. 2005).

The runs used two-way nesting, where NOAH Land Surface Model (LSM) feeds WRF-ARW the surface conditions. WRF then processes the surface conditions, steps forward the new atmospheric conditions, and feeds the new atmospheric data back to NOAH LSM.

The simulations incorporate NOAH LSM using a single layer model for snow. Soil-snow heat flux (G) is the product of thermal diffusivity of snow (K_{snow}) and the differences in skin temperature and the temperature of the first layer over the physical snow depth (Equation 2.4.1.1). Precipitation falls as snow for temperatures below 273 K. The phase changes, accumulations and other energy exchanges occur along the snow-atmosphere and snow-soil boundaries (Chen and Dudhia 2001).

$$G = K_{snow}\frac{T_{skin} - T_{soil}}{D_{snow}} \qquad 2.4.1.1$$

The surface energy balance is determined by shortwave downward radiation plus net longwave radiation equated to the sum of sensible, latent, and snow heat flux (Equation 2.4.1.2). The rate of snow evaporation or sublimation equals potential evaporation when the depth of snow is greater than or equal to potential evaporation over the time step. When the snow depth is less than the potential evaporation, the rate is the depth of the snow divided by the time step (Chen and Dudhia 2001).

$$\begin{aligned}&(1-\alpha)SW\downarrow + LW\downarrow - \sigma T^4\\&= G + \rho_0 C_p C_h |V|(T' - T_a) + \rho_0 L_v C_h |V|(q_s(T') + q_a)\end{aligned} \qquad 2.4.1.2$$

Skin temperature determines if snow phase changes occur. For skin temperatures above 273 K (and snow temperature at 273 K) melting and evaporation or sublimation occur (sublimation or evaporation happen at the potential rate with surface temperature at 273 K). If skin temperature is greater than 273 K snow does not melt (Chen and Dudhia 2001).

The rate of snow melt is calculated from the sum of shortwave down and net longwave radiation at the surface minus sensible, snow and latent heat of evaporation fluxes; therefore the latent heat of fusion and snow melt are added to the right side of the surface energy balance equation when the surface temperature equals or exceeds 273 K.

$$(1-\alpha)SW\downarrow + LW\downarrow - \sigma T^4 = K_{snow}\frac{T_{skin}-T_{soil}}{D_{snow}} + \rho_0 C_p C_h |V|(T_s - T_a) + LE \qquad 2.4.1.3$$

The energy balance equation when the surface temperature equals or exceeds 273 K also alters the temperature difference in the sensible heat flux calculation. The temperature difference is now between the snow temperature and air temperature (instead of skin temperature and air temperature). When snowmelt is greater than the remaining amount of snow left all snowmelts (see Chen and Dudhia 2000, section 3c, for more detail).

2.5 Grid configuration

WRF uses telescope-nested rectangular grids, where each higher-resolution (child) grid must be completely inside a coarser-resolution (parent) grid. For this simulation there were three static telescope-nested domains (the first domain is the outer most parent domain with the second domain being its child and then the parent to the third domain which is the child to the second domain). This simulation used two-way information exchange between fine grid (FG) and course grid (CG). The ratio of horizontal distance and time stepping between the parent domain and the child domain was three-to-one. At every time step the CG forecast is used to calculate the lateral boundary conditions of the FG and then the CG forecast is replaced by the FG.

There are three grid refinement options from the CG. The first option has the FG variables interpolated from the CG. In the second option, which was utilized in

these simulations, the FG variables are input from an external file with greater resolution than the CG. The third option lets nests start at a time after hour zero by using meteorological fields from the CG and then surface static fields from the input file (Skamarock et al. 2008).

WRF uses Arakawa-C grid staggering where velocity components are normal to the sides. All sides of the rectangular course grid have Specified Lateral Boundary Conditions (SLBC). The lateral boundary file is an external file that can be used throughout the simulations to revise the perturbation geopotential, *u* and *v* components of wind, potential temperature, and water vapor.

The CG consists of the specified zone and the relaxed zone. The specified zone for this simulation consists only of the innermost row or column of grid boxes on each side of the child grid. Calculations of the CG are found from external data. In WRF, the relaxed zone is where the model is pushed toward the large-scale forecast (Skamarock et al. 2008). The relaxed zone width in these simulations was four.

2.6 Datasets

U.S. Geological Survey (USGS) topographic and land-use data in WRF are interpreted by geogrid and has twenty-four different land use categories. Starting with the outermost domain to the innermost domain the USGS data were used to create new terrestrial data for each domain at 90, 30, and 15 meters respectively.

The data used in the preprocessing step was NCEP/NCAR Global Reanalysis Products from NCAR with a temporal resolution of six hours and spatial resolution T62 (209km) with 17 pressure-levels (28 vertical sigma-levels). The output format is WMO GRIB DATA. The dataset was published and created by the Data Support Section Division of NCAR.

Chapter 3

DIRECT EFFECTS

3.1 Albedo and surface shortwave radiation flux

3.1.1 Albedo

The modeled albedos in all cases are in agreement with typical Northern Hemisphere snow and snow-free albedos (Cohen and Rind 1991; Klingaman et al. 2008; Kung et al. 1964; Robinson and Kukla 1985). The average Northeast land cover albedo of the snowpack simulation is 0.64 and is more than two times the average snow-free albedo of 0.31 (Table 3.1.1). The average albedo differences between the snowpack and the snow-free simulations are spatially consistent and range from 0.28 to 0.36 (Figure 3.8.1 and Table 3.1.1). Differences in the text refer to variations between the snowpack and snow-free simulations, subtracting the snow-free simulation from the snowpack simulation. In addition, differences and averages will be calculated from values over the Northeast landmass unless otherwise stated.

Table 3.1.1: Average Northeast surface albedos for the snowpack and snow-free simulations of the 8-10 February 1969, 25-28 December 1969, 18-20 February 1972, 12-14 March 1993, and, 24-26 January 2000.

	Snowpack				Snow-free			
	Average	Maximum	Minimum	Standard Deviation	Average	Maximum	Minimum	Standard Deviation
Feb-69	0.63	0.80	0.23	0.06	0.27	0.80	0.12	0.14
Dec-69	0.62	0.80	0.45	0.05	0.28	0.80	0.12	0.10
Feb-72	0.64	0.80	0.44	0.07	0.33	0.80	0.12	0.17
Mar-93	0.65	0.80	0.48	0.07	0.37	0.80	0.12	0.20
Jan-00	0.64	0.80	0.51	0.07	0.31	0.80	0.12	0.17
Average	0.64	0.80	0.42	0.06	0.31	0.80	0.12	0.16

	Difference (Snow - Snow-free)			
	Average	Maximum Negative	Maximum Positive	Standard Deviation
Feb-69	0.36	-0.02	0.59	0.11
Dec-69	0.35	-0.01	0.59	0.11
Feb-72	0.32	0.00	0.59	0.14
Mar-93	0.28	-0.03	0.58	0.16
Jan-00	0.33	-0.02	0.58	0.14
Average	0.33	-0.02	0.58	0.13

3.1.2 Downward shortwave radiation surface flux

In the snow covered and no-snow simulations, the average downward shortwave surface flux is around 160 W m^{-2}, with an average difference of only 5.3 W m^{-2} (Table 3.1.2). The greater average downward shortwave flux of the snowpack simulations may indicate that the snowpack simulations have less cloud cover. The average magnitude of incoming shortwave radiation in both simulations increases with storms later in the nor'easter season. Later season storms have longer days and greater insolation; therefore the magnitude of incoming shortwave radiation has a seasonal trend. In contrast, the difference in magnitudes between simulations do not follow a seasonal trend.

3.1.3 Reflected shortwave radiation

The average upward shortwave radiation of the snowpack simulations during daylight hours is -107.7 W m^{-2} which is double the magnitude of the upward shortwave radiation of the snow-free simulations at -51.4 W m^{-2} (Figure 3.8.3). All fluxes directed up from the surface are reported as negative values. The average difference between the reflected shortwave radiation in the snow and snow-free simulations is -56.3 W m^{-2} (Table 3.1.3).

In the snow simulations, the order of magnitude of the reflected shortwave radiation follows the seasonality of incoming solar radiation where the later season storms have a greater reflected shortwave radiation compared to storms earlier in the season. The order of magnitude of reflected shortwave radiation in the snow-free simulations are closely related, but not directly, related to the seasons. The March storm has the largest magnitude of reflected shortwave radiation and the December

storm has the smallest. The order of magnitude of the differences in reflected shortwave radiation follows the same trend (Table 3.1.3).

3.1.4 Net shortwave radiation

The net shortwave radiation is the sum of the upwelling and downwelling shortwave radiation at the surface. The average net shortwave radiation at the surface of the snow simulations is approximately half the average of the snow-free simulations at 59.7 and 110.7 W m^{-2}, respectively (Table 3.1.4). The magnitudes of the difference in net shortwave radiation is essentially the difference in magnitudes of the reflected shortwave radiation because the downward shortwave radiation is approximately the same between simulations and the net shortwave radiation is simply the sum of the downward and upward shortwave radiation. The average difference of net shortwave radiations is 51.0 W m^{-2} and the average difference of the reflected shortwave radiations is 56.3 W m^{-2}.

Table 3.1.2: Downward shortwave radiation surface flux (W m^{-2}) over the Northeast for the snowpack and snow-free simulations of the 8-10 February 1969, 25-28 December 1969, 18-20 February 1972, 12-14 March 1993, and, 24-26 January 2000.

	Snow Simulation			Snow-free Simulation		
	Average	Maximum	Standard Deviation	Average	Maximum	Standard Deviation
Feb-69	184.7	707.7	186.3	187.0	706.4	187.6
Dec-69	85.9	540.5	112.0	84.3	539.0	109.7
Feb-72	158.8	759.0	170.8	155.2	757.8	164.0
Mar-93	248.8	897.1	242.8	233.4	893.0	226.3
Jan-00	158.8	640.9	159.4	150.5	631.7	153.6
Average	167.4	709.0	174.3	162.1	705.6	168.2

	Difference (Snow - Snow-free)			
	Average	Maximum Negative	Maximum Positive	Standard Deviation
Feb-69	-2.3	-595.5	543.1	58.8
Dec-69	1.6	-288.2	401.9	28.6
Feb-72	3.6	-581.1	593.7	54.0
Mar-93	15.4	-602.2	642.0	59.3
Jan-00	8.3	-427.5	362.6	48.2
Average	5.3	-498.9	508.7	49.8

Table 3.1.3: Reflected shortwave radiation (W m^{-2}) over the Northeast for the snowpack and snow-free simulations of the 8-10 February 1969, 25-28 December 1969, 18-20 February 1972, 12-14 March 1993, and, 24-26 January 2000.

	Snow Simulation			Snow-free Simulation		
	Average	Maximum	Standard Deviation	Average	Maximum	Standard Deviation
Feb-69	-117.4	-470.6	120.0	-51.1	-413.3	59.8
Dec-69	-54.7	-336.7	72.5	-24.3	-288.1	35.5
Feb-72	-103.3	-523.9	113.1	-49.3	-450.0	70.5
Mar-93	-161.5	-614.7	159.7	-89.0	-601.3	114.1
Jan-00	-101.6	-421.1	102.7	-43.3	-347.8	50.1
Average	-107.7	-473.4	113.6	-51.4	-420.1	66.0

	Difference (Snow - Snow-free)			
	Average	Maximum Negative	Maximum Positive	Standard Deviation
Feb-69	-66.3	-402.7	147.0	76.9
Dec-69	-30.4	-269.6	98.6	44.2
Feb-72	-54.1	-420.2	191.6	73.1
Mar-93	-72.5	-523.6	481.8	93.4
Jan-00	-58.3	-316.7	269.9	67.7
Average	-56.3	-386.6	237.8	71.1

Table 3.1.4: Net shortwave radiation (W m^{-2}) over the Northeast for the snowpack and snow-free simulations of the 8-10 February 1969, 25-28 December 1969, 18-20 February 1972, 12-14 March 1993, and, 24-26 January 2000.

	Snow Simulation			Snow-free Simulation		
	Average	Maximum	Standard Deviation	Average	Maximum	Standard Deviation
Feb-69	67.3	520.1	69.7	135.9	585.2	140.8
Dec-69	31.2	222.5	40.7	60.1	376.1	78.3
Feb-72	55.5	370.1	61.5	105.9	626.1	119.5
Mar-93	87.3	448.0	88.9	144.4	662.3	150.5
Jan-00	57.1	275.8	59.2	107.1	510.6	115.5
Average	59.7	367.3	64.0	110.7	552	120.9

	Difference (Snow - Snow-free)			
	Average	Maximum Negative	Maximum Positive	Standard Deviation
Feb-69	-68.6	-233.8	494.2	81.7
Dec-69	-28.8	-132.3	290.7	42.9
Feb-72	-50.4	-241.4	493.5	67.3
Mar-93	-57.1	-241.4	469.9	78.4
Jan-00	-50.0	-129.3	391.6	64.4
Average	-51.0	-195.6	428.0	66.9

3.2 Longwave radiation flux

3.2.1 Downward longwave surface flux

The average downward longwave surface fluxes of the snowpack simulations are reduced over the entire Northeast United States and Southeast Canada (Figure 3.8.4 and Table 3.2.1). The average downward longwave surface flux is 235.7 W m^{-2} in the snowpack simulations and 244.9 W m^{-2} in the snow-free simulation. The amount of downward longwave radiation is determined by the amount of moisture present in the atmosphere. Decreasing the atmospheric moisture reduces the longwave radiation reradiated downward toward the surface; therefore the snowpack simulations will typically have less downward longwave flux because the near-surface atmosphere is cooler and drier.

3.2.2 Outgoing longwave radiation at the top of the atmosphere

On average, less outgoing longwave radiation (OLR) leaves the top of the atmosphere (TOA) for the snowpack simulations than for the snow-free simulations by almost 4.0 W m^{-2} (Table 3.2.2, Figure 3.8.5). The average OLR of the snowpack simulations is approximately 185 W m^{-2}. Differences in the OLR at the TOA are due to either changes in cloud cover or the insulating effect of snow.

Snow insulates and traps longwave radiation from the ground decreasing the amount of OLR. Increasing cloud cover will enhance the insulating effect of snow by trapping more OLR. Decreasing cloud cover results in more OLR escaping and could therefore negate the effect of snow insulation. The net loss in OLR at the TOA in the snowpack simulations is an indication that the cloud effect is smaller than the insulation from the snowpack or working in conjunction with the snowpack insulation;

however in these simulations there is not a significant difference in the total cloud cover between the snowpack and snow-free simulation; therefore the decrease in OLR in the snowpack simulations can be attributed to either the insulating effect of the snowpack or the decrease in available energy at the surface of the earth.

3.2.3 Net longwave radiation

The net surface longwave radiation was calculated based on Hartman (1994) equation 4.14. The net longwave radiation is the difference between the downwelling radiation and the blackbody emission of the surface multiplied by the surface emissivity (equation 3.2.3). The average net longwave radiation of the snowpack simulations is -24.9 W m^{-2} and the snow-free average is -36.1 W m^{-2} where the negative values represent a loss of longwave radiation from the surface or upward flux. (Table 3.2.3). Therefore the snowpack simulation emits less longwave radiation at the surface, which is congruent with lower surface temperatures.

$$Net\ LWR = \varepsilon(DLR - \sigma T_s^4) \qquad 3.2.3$$

Table 3.2.1: Downward surface longwave flux (W m^{-2}) over the Northeast for the snowpack and snow-free simulations of the 8-10 February 1969, 25-28 December 1969, 18-20 February 1972, 12-14 March 1993, and, 24-26 January 2000.

	Snowpack				Snow-free			
	Average	Minimum	Maximum	Standard Deviation	Average	Minimum	Maximum	Standard Deviation
Feb-69	247.4	147.1	378.0	48.9	250.4	157.8	386.0	49.0
Dec-69	242.2	138.4	375.0	48.3	247.4	148.2	377.1	48.2
Feb-72	247.0	106.6	377.4	54.4	255.2	108.6	380.5	54.0
Mar-93	217.5	112.5	404.6	53.7	234.3	120.6	409.8	49.1
Jan-00	224.2	128.1	381.4	49.4	237.0	137.1	381.3	46.8
Average	235.7	126.5	383.3	50.9	244.9	134.4	386.9	49.4

	Difference (Snow - Snow-free)			
	Average	Maximum Negative	Maximum Positive	Standard Deviation
Feb-69	-3.1	-114.2	97.5	21.6
Dec-69	-5.2	-105.8	102.5	17.6
Feb-72	-8.1	-122.5	103.0	19.3
Mar-93	-16.8	-129.1	100.2	25.0
Jan-00	-12.8	-116.6	102.5	25.8
Average	-9.2	-117.6	101.1	21.9

Table 3.2.2: Outgoing longwave radiation at the top of the atmosphere (W m^{-2}) over the Northeast for the snowpack and snow-free simulations of the 8-10 February 1969, 25-28 December 1969, 18-20 February 1972, 12-14 March 1993, and, 24-26 January 2000.

	Snowpack				Snow-free			
	Average	Minimum	Maximum	Standard Deviation	Average	Minimum	Maximum	Standard Deviation
Feb-69	187.4	110.3	270.2	33.5	191.6	113.1	276.8	36.0
Dec-69	189.2	120.2	257.7	27.5	192.4	121.6	257.2	28.7
Feb-72	184.9	125.1	270.3	26.7	187.2	123.3	270.4	28.1
Mar-93	171.6	102.7	281.6	29.4	175.7	104.3	275.2	31.8
Jan-00	190.8	100.6	273.6	25.1	196.3	100.9	275.3	26.7
Average	184.8	111.8	270.7	28.4	188.6	112.6	271.0	30.3

	Difference (Snow - Snow-free)			
	Average	Maximum Negative	Maximum Positive	Standard Deviation
Feb-69	-4.2	-120.0	117.7	16.2
Dec-69	-3.2	-106.0	104.9	9.5
Feb-72	-2.3	-98.2	107.2	17.4
Mar-93	-4.1	-130.4	138.9	13.5
Jan-00	-5.6	-133.6	139.2	18.8
Average	-3.9	-117.7	121.6	15.1

Table 3.2.3: Average net longwave radiation (W m^{-2}) over the Northeast for the snowpack and snow-free simulations of the 8-10 February 1969, 25-28 December 1969, 18-20 February 1972, 12-14 March 1993, and, 24-26 January 2000.. Calculated using modeled skin temperature, emissivity and downward longwave radiation. Calculated using Hartman (1994) equation 4.14.

	Snow	Snow-Free	Difference
Feb-69	-26.3	-41.8	15.6
Dec-69	-21.8	-32.9	11.1
Feb-72	-16.5	-24.9	8.4
Mar-93	-28.8	-39.1	10.3
Jan-00	-31.3	-42.4	11.0
Average	-24.9	-36.1	11.2

3.3 Upward sensible heat flux

The average upward sensible heat flux is negative in the snowpack simulations and is positive in the snow-free simulations (Table 3.3.1). The December 1969 case is the only exception. Since sensible heat flux is defined with upward direction from the surface a negative flux indicates that the sensible heat flux is directed toward the surface and that the ground temperature is cooler than the overlaying atmosphere and for positive sensible heat flux the ground temperature is warmer than the air temperature. The snowpack simulations have an average sensible heat flux of -13.0 W m^{-2} and the snow-free have an average sensible heat flux of 8.0 W m^{-2}.

Examining the sensible heat flux spatially, the snowpack simulations have decreased average sensible heat fluxes over Nova Scotia and the Middle Atlantic west through Ohio. Excluding the 1969 cases the decreased snowpack values also occur in inland Canada (Figure 3.8.6, Table 3.3.1).

The snowpack simulations has larger differences in average sensible heat fluxes off the Atlantic Coast and over the Great Lakes compared to the snow-free simulations (Figure 3.8.6). The temperature of the Atlantic is the same in both simulations. Both simulations advect colder continental offshore air over the warmer Atlantic. The air over the snowpack simulations is cooler creating a larger positive sensible heat flux, since the contrast between the warm water and colder air is greater.

Sensible heat flux varies with vertical temperature profile and the square of surface wind speed. Since there is little to no difference in surface wind speed the differences in the sensible heat flux between the maximum and minimum run is strictly due to the vertical temperature profile. Snow-free ground conditions in these simulations usually have temperatures above air temperatures and positive upward

sensible heat flux. Snow cover insulates the ground with a layer that will not go above 0°C, usually reducing the sensible heating of the atmosphere by the ground.

Table 3.3.1: Upward sensible heat flux (W m-2) over the Northeast for the snowpack and snow-free simulations of the 8-10 February 1969, 25-28 December 1969, 18-20 February 1972, 12-14 March 1993, and, 24-26 January 2000.

	Snowpack				Snow-free			
	Average	Maximum	Minimum	Standard Deviation	Average	Maximum	Minimum	Standard Deviation
Feb-69	-16.1	-532.8	238.6	41.7	0.1	-526.5	350.1	43.6
Dec-69	-21.7	-693.2	78.4	38.2	-11.6	-364.9	164.5	29.9
Feb-72	-16.5	-669.2	152.6	42.0	15.9	-222.7	422.2	58.4
Mar-93	-1.8	-1056.4	207.0	59.1	26.6	-796.9	416.5	83.6
Jan-00	-8.9	-731.8	122.4	34.7	9.2	-600.8	246.4	43.0
Average	-13.0	-736.7	159.8	43.1	8.0	-502.4	320.0	51.7

	Difference (Snow - Snow-free)			
	Average	Maximum Negative	Maximum Positive	Standard Deviation
Feb-69	-16.2	-484.0	399.3	35.7
Dec-69	-10.1	-610.5	194.3	22.4
Feb-72	-32.3	-718.9	193.7	45.1
Mar-93	-28.4	-917.3	771.4	42.6
Jan-00	-18.0	-517.3	103.9	26.0
Average	-21.0	-649.6	332.5	34.3

3.4 Ground heat flux

The average ground heat flux, the heat flux from the surface into the ground, is -3.1 W m^{-2} in the snow simulations and -12.2 W m^{-2} in the snow-free simulation (Table 3.4.1). Spatially, there is less average ground heat flux for the snowpack simulations in the Northeast compared to the snow-free simulations, excluding Maine, New Brunswick, and Nova Scotia (Figure 3.8.7). The ground heat flux is expected to be reduced in magnitude for the snow conditions because the snowpack is acting as an insulator. In the South, the snowpack and snow-free simulations have similar ground heat flux values, with the exception of the January 2000 case.

Table 3.4.1: Ground heat flux (W m^{-2}) over the Northeast for the snowpack and snow-free simulations of the 8-10 February 1969, 25-28 December 1969, 18-20 February 1972, 12-14 March 1993, and, 24-26 January 2000.

	Snow				Snow-free			
	Average	Minimum	Maximum	Standard Deviation	Average	Minimum	Maximum	Standard Deviation
Feb-69	-2.8	-104.4	74.7	6.2	-0.1	-139.0	312.8	52.1
Dec-69	-2.1	-21.8	26.6	2.9	-10.4	-172.1	265.2	32.6
Feb-72	-3.9	-181.3	25.6	5.4	-21.4	-341.7	265.2	51.0
Mar-93	-4.1	-42.3	21.1	3.6	-21.5	-247.0	283.2	43.7
Jan-00	-2.7	-24.3	17.9	3.2	-7.8	-167.9	262.9	43.3
Average	-3.1	-74.8	33.2	4.2	-12.2	-213.5	277.8	44.5

	Difference			
	Average	Maximum Negative	Maximum Positive	Standard Deviation
Feb-69	-2.7	-314.5	122.4	49.7
Dec-69	8.4	-253.8	163.3	30.8
Feb-72	17.5	-270.7	327.3	48.4
Mar-93	17.4	-272.3	240.1	41.7
Jan-00	5.2	-262.1	161.6	41.4
Average	9.1	-274.7	202.9	42.4

3.5 Latent heat flux

The average latent heat flux is 11.9 W m^{-2} for the snowpack simulations and 14.7 W m^{-2} for the snow-free simulations; therefore the average upward latent heat flux is 2.8 W m^{-2} less in the snowpack simulations (Table 3.5.1). The reduced latent heat flux values in the snowpack mainly occur inland (Figure 3.8.8). In all the simulations, the latent heat flux over the ocean is greater in the snowpack simulation. Like sensible heat flux, latent heat flux is dependent on the vertical potential temperature profile and the square of magnitude of surface wind speed; therefore with little to no difference in surface wind speed the differences in latent heat flux between the maximum and minimum run is strictly due to the vertical temperature profile. The decreased latent heat flux over the ocean may be an expansion of the land-atmosphere snow cover effects displaced over the ocean. The ocean temperature is constant in the simulations therefore the air over the ocean in the snowpack simulations must be drier or cooler than the air in the snow-free simulations.

Hourly latent heat flux maps showed a maximum at 1800 UTC (1 pm EST), nearly the warmest time of the day and corresponding to the greatest solar insulation which would lead to snow melting, which is a latent heat sink.

Table 3.5.1: Latent heat flux (W m^{-2}) over the Northeast for the snowpack and snow-free simulations of the 8-10 February 1969, 25-28 December 1969, 18-20 February 1972, 12-14 March 1993, and, 24-26 January 2000.

	Snowpack				Snow-free			
	Average	Maximum	Minimum	Standard Deviation	Average	Maximum	Minimum	Standard Deviation
Feb-69	12.0	-27.9	251.4	22.5	13.3	-163.3	539.8	23.7
Dec-69	8.2	-26.4	215.4	16.2	8.5	-134.0	143.8	13.3
Feb-72	18.8	-33.8	423.6	20.9	20.3	-53.6	185.8	20.9
Mar-93	14.7	-23.1	463.8	23.6	22.2	-141.5	358.8	25.9
Jan-00	6.1	-28.5	240.3	15.1	9.4	-138.2	161.8	14.7
Average	11.9	-27.9	318.9	19.7	14.7	-126.1	278.0	19.7

	Difference (Snow - Snow-free)			
	Average	Maximum Negative	Maximum Positive	Standard Deviation
Feb-69	-1.4	-458.4	259.0	17.3
Dec-69	-0.3	-85.5	228.7	9.3
Feb-72	-1.5	-163.2	352.1	16.4
Mar-93	-7.6	-224.9	397.3	11.1
Jan-00	-3.4	-125.2	238.7	10.2
Average	-2.8	-211.4	295.2	12.9

3.6 Net surface energy budget

On average, the net surface energy budget is reduced by 54.4 W m^{-2}. The surface energy balance difference is the sum of the differences in surface sensible heat flux (-21.0 W m^{-2}), latent heat flux (-2.8 W m^{-2}), net shortwave radiation (-51.0 W m^{-2}), net longwave radiation (11.2 W m^{-2}), and ground heat flux (9.1 W m^{-2}).

Sensible heat flux and net shortwave radiation are the largest contributors to the reduction in the net surface energy followed by ground heat flux and latent heat flux. The net longwave radiation and ground heat flux counter act the reduction of all the other terms by creating a slight gain in the net surface energy for the snowpack simulation.

It is logical that the snowpack creates a reduction in the surface energy because the snowpack i) increases albedo which increases the reflected shortwave radiation, ii) has a cooler surface decreasing sensible heat flux, and iii) insulates the heat energy coming from the land reducing the ground heat flux.

It is expected the snowpack simulations will have reduced near-surface temperatures due to the decrease in the surface energy.

3.7 Temperature

3.7.1 Skin temperature and two-meter temperature

The average two-meter temperature and average skin temperature are both cooler in the snowpack simulation. In the snowpack simulation, the average skin temperature is -12.3°C and the average two-meter temperature is -11.6 °C, while in the snow-free simulations the average skin temperature is -7.1°C and the average two-meter temperature is -7.2 °C (Tables 3.7.1 and 3.7.2). The cooling in the snowpack

simulations is greater for the skin temperature than the two-meter temperature (-5.2°C versus -4.4°C).

The two-meter temperature over the Northeast landmass and slightly east into the Atlantic are always less in the snowpack simulations compared to the snow-free simulations (Figure 3.8.9). The cooler surface temperatures are due to the reduction in available energy at the surface of the snowpack simulations compared to the snow-free simulations (Section 3.6). The cooler skin temperatures of the snowpack simulations created negative sensible heat fluxes, as discussed previously, so the cooling here is consistent with the above discussion of the surface energy balance components.

3.7.2 Near surface temperature gradient

The difference in skin temperature and two-meter temperature is an indication of the near-surface temperature gradient. The average difference between the skin temperature and two-meter temperature is -0.7°C for the snow simulations and 0.1°C for the snowpack simulations (Table 3.7.3); In the snowpack simulations, the ground temperature is less than the air above and in the snow-free simulations the ground temperature is greater than the overlaying air mass.

The ocean is not influenced by the atmospheric conditions in the simulations; therefore the average sea surface temperature of the Atlantic Ocean adjacent to the Northeast United States is 9.8°C in both simulations (Table 3.7.4). Atmospheric conditions are influenced by the ocean and land surfaces. The average two-meter temperature gradient over the adjacent Atlantic is 6.4°C for the snowpack simulations and 7.0°C for the snow-free simulations (Table 3.7.5); therefore the near-surface temperature gradient over the Atlantic is positive in both simulations but the gradient is greater for the snowpack simulations. The sign of the near-surface temperature

gradient is the same in both simulations over the Atlantic and different over the Northeast land surface, but the magnitude of differences in the simulation's near-surface temperature gradient is larger over the Atlantic (Tables 3.7.3 and 3.7.5).

3.7.3 Boundary layer temperature gradient

Temperature differences at increasing η-levels determine how high temperature depressions associated with the snowpack extend upward into the troposphere. When referring to η-levels it should be noted that the η-levels are really η multiplied by 1000; a value commonly used since it corresponds well to pressure levels. The average magnitude of the temperature differences between the snowpack simulations decreases by 0.5°C per decrease in η-level until η of approximately 800 (Table 3.7.6 and Figure 3.8.10).

Table 3.7.1: Skin temperature for Northeast (°C) for the snowpack and snow-free simulations of the 8-10 February 1969, 25-28 December 1969, 18-20 February 1972, 12-14 March 1993, and, 24-26 January 2000.

	Snow				Snow-free			
	Average	Minimum	Maximum	Standard Deviation	Average	Maximum Negative	Maximum Positive	Standard Deviation
Feb-69	-9.1	-35.0	7.1	7.4	-4.4	-29.6	19.5	5.7
Dec-69	-11.5	-39.3	3.1	7.4	-7.3	-29.6	11.4	5.0
Feb-72	-11.7	-45.4	5.6	9.5	-7.5	-39.6	19.2	8.5
Mar-93	-15.9	-45.3	5.9	8.4	-8.9	-39.0	17.7	5.8
Jan-00	-13.5	-43.2	1.4	8.1	-7.4	-37.6	9.8	5.4
Average	-12.3	-41.6	4.6	8.2	-7.1	-35.1	15.5	6.1

	Differences			
	Average	Minimum	Maximum	Standard Deviation
Feb-69	-4.7	-23.3	10.8	4.1
Dec-69	-4.1	-22.9	7.4	3.7
Feb-72	-4.2	-26.4	10.4	3.3
Mar-93	-6.9	-30.3	9.1	4.5
Jan-00	-6.1	-28.8	9.1	4.5
Average	-5.2	-26.3	9.4	4.0

Table 3.7.2: Temperature at two meters for Northeast (°C) for the snowpack and snow-free simulations of the 8-10 February 1969, 25-28 December 1969, 18-20 February 1972, 12-14 March 1993, and, 24-26 January 2000.

	Snow				Snow-free			
	Average	Minimum	Maximum	Standard Deviation	Average	Maximum Negative	Maximum Positive	Standard Deviation
Feb-69	-8.2	-32.0	9.5	6.8	-4.2	-25.4	15.6	5.1
Dec-69	-10.4	-38.3	9.8	6.8	-6.9	-25.3	12.7	4.7
Feb-72	-11.2	-43.7	9.7	9.5	-7.8	-37.7	15.6	8.4
Mar-93	-15.5	-42.1	14.5	7.9	-9.6	-34.5	19.8	5.8
Jan-00	-12.7	-40.1	9.7	7.4	-7.6	-33.4	12.0	5.0
Average	-11.6	-39.2	10.6	7.7	-7.2	-31.2	15.1	5.8

	Differences			
	Average	Minimum	Maximum	Standard Deviation
Feb-69	-4.0	-20.3	7.9	3.3
Dec-69	-3.5	-23.9	7.1	3.1
Feb-72	-3.4	-22.1	7.6	2.7
Mar-93	-6.0	-26.7	9.9	3.6
Jan-00	-5.1	-25.3	8.3	3.8
Average	-4.4	-23.7	8.1	3.3

Table 3.7.3: Near-surface temperature gradient (skin minus two-meter temperature) over the Northeast United States (°C) for the snowpack and snow-free simulations of the 8-10 February 1969, 25-28 December 1969, 18-20 February 1972, 12-14 March 1993, and, 24-26 January 2000.

	Snow	Snow-Free	Difference
Feb-69	-0.9	-0.2	-0.7
Dec-69	-1.0	-0.5	-0.6
Feb-72	-0.5	0.2	-0.7
Mar-93	-0.3	0.7	-1.0
Jan-00	-0.8	0.2	-1.0
Average	-0.7	0.1	-0.8

Table 3.7.4: Sea surface temperature for Atlantic Ocean adjacent to the Northeast United States (°C) for the snowpack and snow-free simulations of the 8-10 February 1969, 25-28 December 1969, 18-20 February 1972, 12-14 March 1993, and, 24-26 January 2000.

	Snow and Snow-free Values			
	Average	Minimum	Maximum	Standard Deviation
Feb-69	8.9	-2.1	18.9	6.4
Dec-69	10.6	0.9	19.9	6.1
Feb-72	9.1	-2.1	19.7	6.8
Mar-93	9.6	-2.1	19.3	7.0
Jan-00	10.8	-2.1	20.2	6.5
Average	9.8	-1.5	19.6	6.6

Table 3.7.5: Near-surface temperature gradient (skin minus two-meter temperature) over the Atlantic Ocean adjacent to the Northeast United States (°C) for the snowpack and snow-free simulations of the 8-10 February 1969, 25-28 December 1969, 18-20 February 1972, 12-14 March 1993, and, 24-26 January 2000.

	Snow	Snow-Free	Difference
Feb-69	3.0	2.5	0.5
Dec-69	3.7	3.3	0.3
Feb-72	3.3	2.7	0.7
Mar-93	4.4	3.5	0.9
Jan-00	2.4	2.0	0.4
Average	3.4	2.8	0.6

Table 3.7.6: Temperature difference (snowpack-snow-free) over the northeast landmass (°C) averaged over storm duration for the snowpack and snow-free simulations of the 8-10 February 1969, 25-28 December 1969, 18-20 February 1972, 12-14 March 1993, and, 24-26 January 2000.

η	997				885			
	Average	Maximum Negative	Maximum Positive	Standard deviation	Average	Maximum Negative	Maximum Positive	Standard deviation
Feb-69	-3.4	-18.6	4.8	2.6	-0.2	-5.8	4.1	0.5
Dec-69	-3.0	-24.4	7.1	2.5	-0.1	-4.6	3.5	0.4
Feb-72	-3.2	-22.4	4.7	2.5	-0.8	-10.4	4.9	1.1
Mar-93	-5.4	-23.9	14.2	2.9	-0.6	-12.0	15.6	1.1
Jan-00	-4.4	-22.6	12.0	3.1	-0.4	-7.3	6.5	0.7
Average	-3.9	-22.4	8.6	2.7	-0.4	-8.0	6.9	0.8

η	704				479			
	Average	Maximum Negative	Maximum Positive	Standard deviation	Average	Maximum Negative	Maximum Positive	Standard deviation
Feb-69	-0.1	-3.6	3.5	0.4	0.0	-2.7	3.6	0.3
Dec-69	0.1	-2.7	3.0	0.3	0.0	-3.3	2.5	0.2
Feb-72	-0.2	-7.5	5.7	0.8	-0.1	-5.1	4.3	0.6
Mar-93	0.0	-6.0	11.8	0.8	0.2	-3.8	3.6	0.6
Jan-00	0.0	-3.4	6.1	0.5	0.1	-2.4	2.9	0.3
Average	-0.1	-4.6	6.0	0.6	0.0	-3.4	3.4	0.4

3.8 Direct effects summary

The direct effects of the snowpack are as anticipated; there is a decrease in the net surface energy mainly from an increase in reflected shortwave radiation that leads to a reduction in the near surface temperature. The direct atmospheric changes set the stage for the indirect effects discussed in the next chapter.

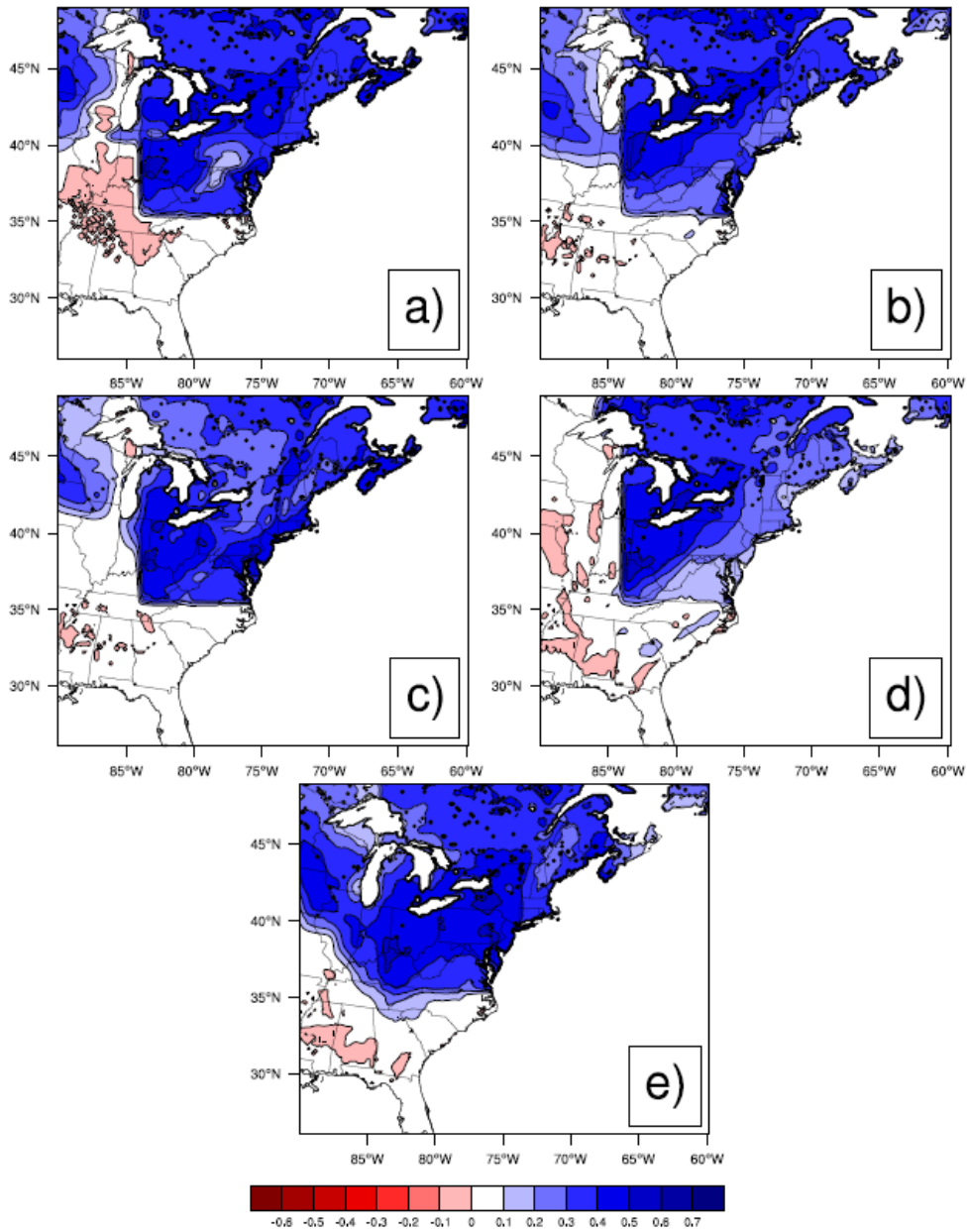

Figure 3.8.1: Average storm duration surface albedo differences smoothed using a 9 point average. a) February 1969 b) December 1969 c) February 1972 d) March 1993 e) January 2000. Contours by 0.1 from -0.6 to 0.7.

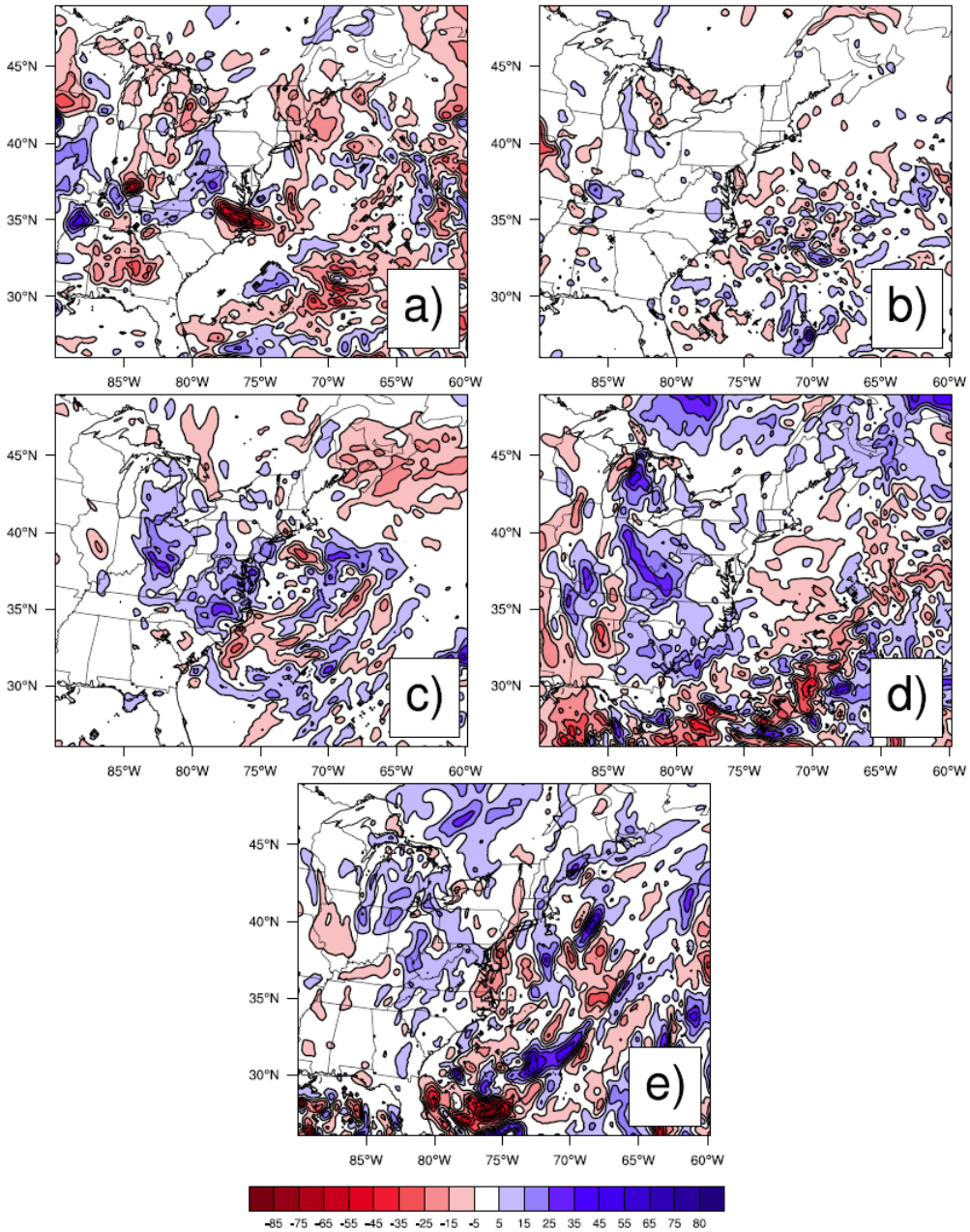

Figure 3.8.2: Average storm duration difference in downward shortwave radiation smoothed using 9 point average. a) February 1969 b) December 1969 c) February 1972 d) March 1993 e) January 2000. Contoured by 0.1 from -80.0 to 85.0 W m^{-2} by 15.0 W m^{-2}.

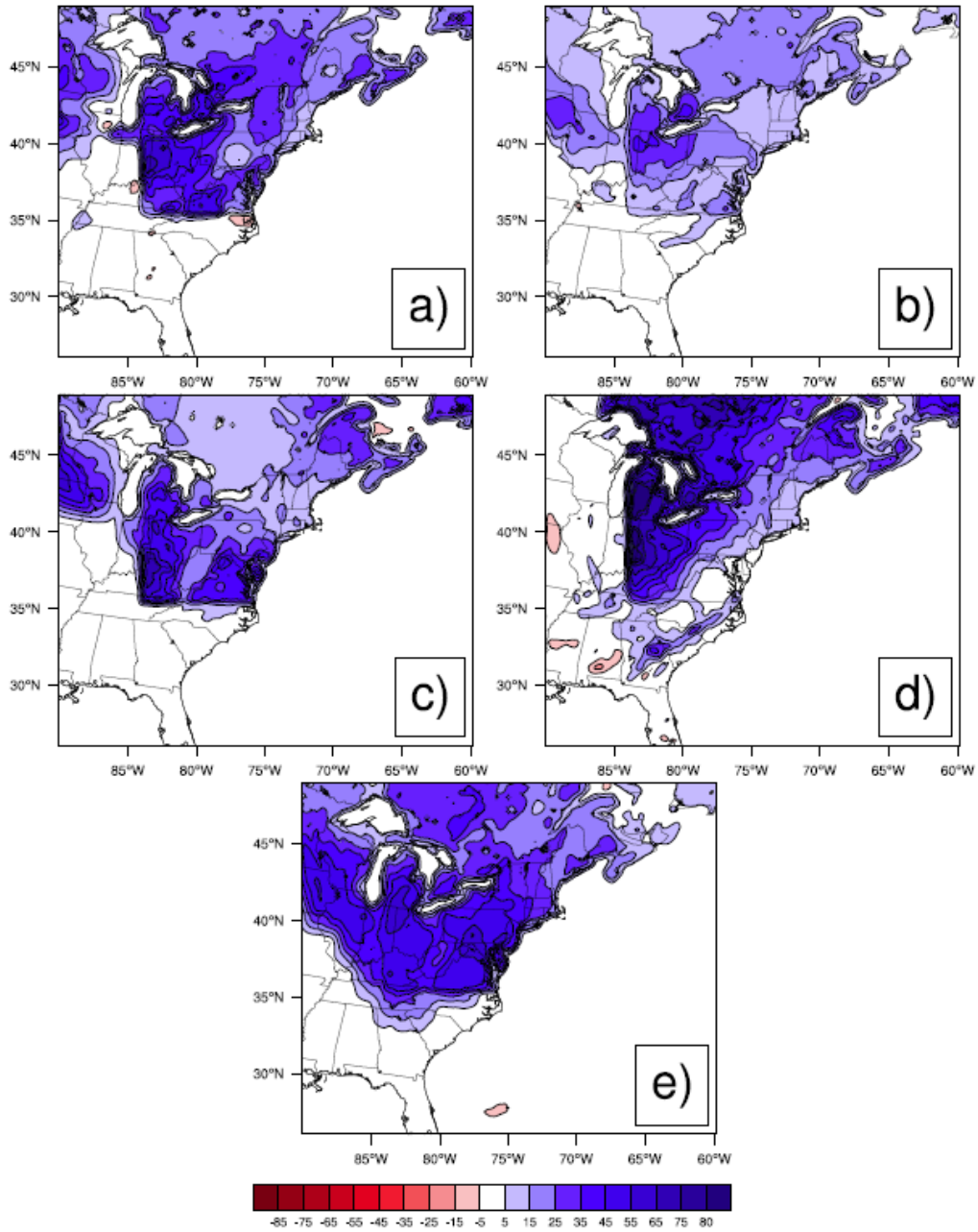

Figure 3.8.3: Average storm duration difference in upward shortwave radiation smoothed using 9 point average. a) February 1969 b) December 1969 c) February 1972 d) March 1993 e) January 2000. Contoured by 15.0 from -80.0 to 85.0 W m^{-2}.

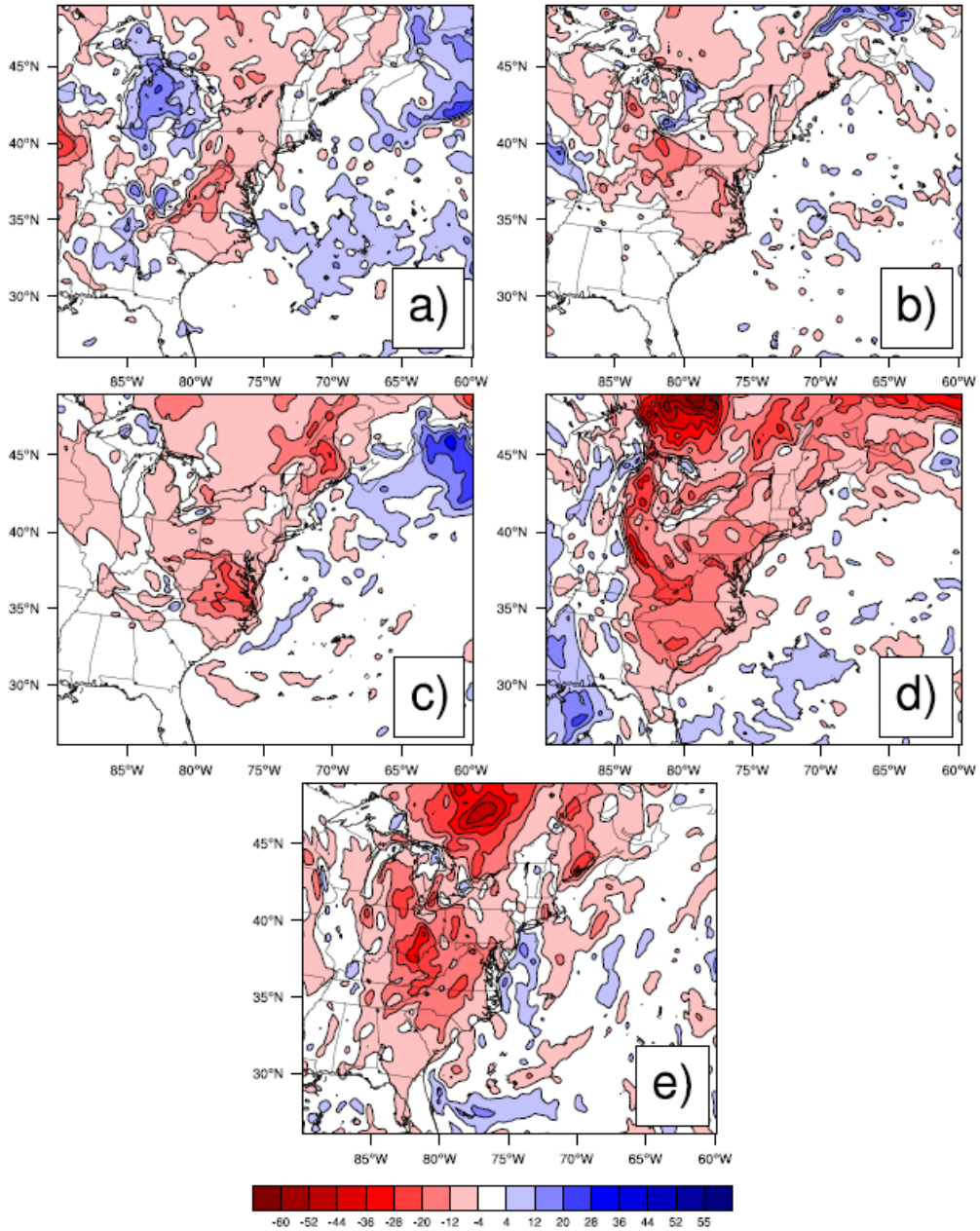

Figure 3.8.4: Average storm duration difference in downward longwave flux at the surface smoothed using a 9 point average. a) February 1969 b) December 1969 c) February 1972 d) March 1993 e) January 2000. Contoured by 8.0 from -60.0 to 55.0 W m^{-2}.

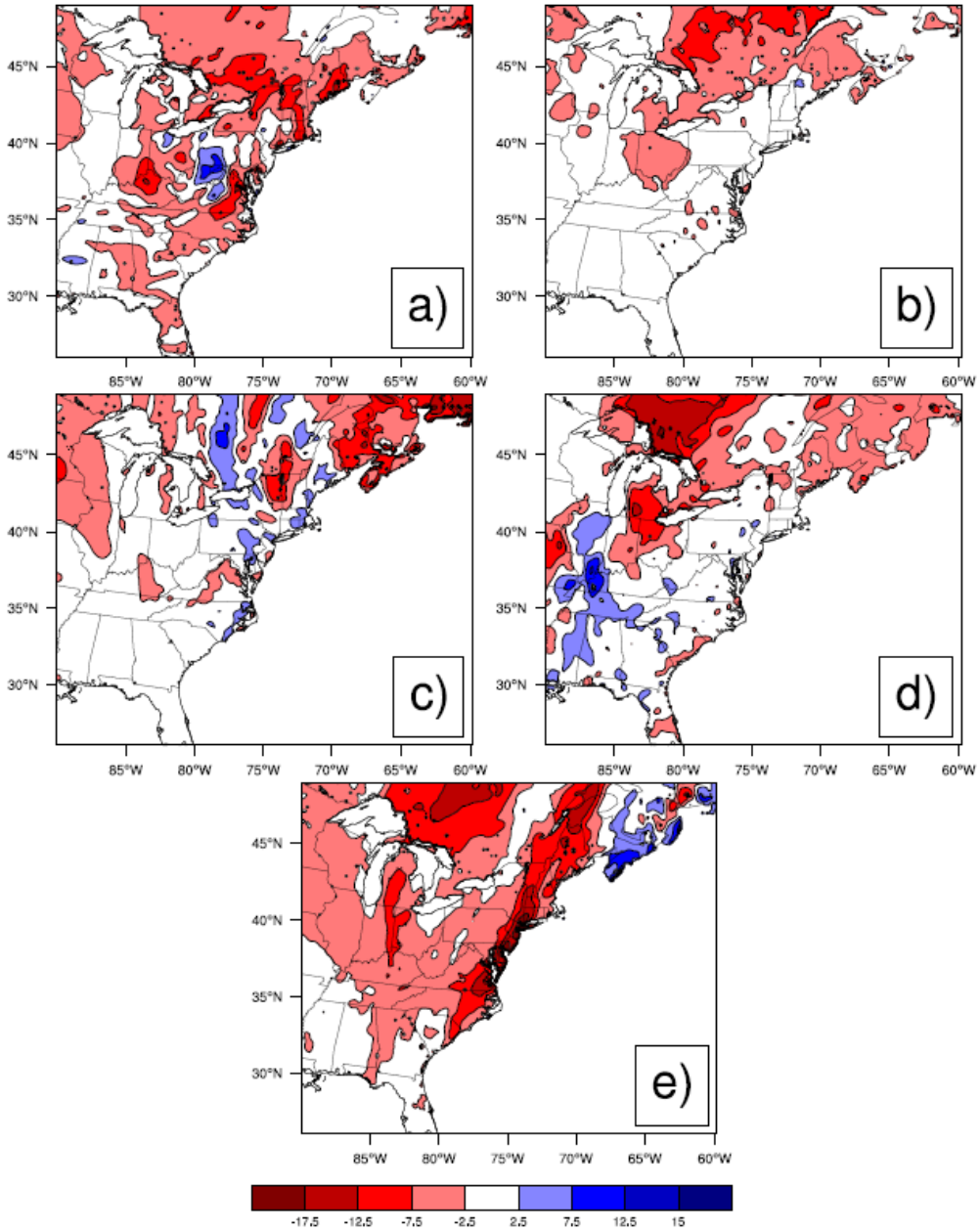

Figure 3.8.5: Average difference in OLR at the top of the atmosphere over storms duration smoothed using 9 point average with landmask. a) February 1969 b) December 1969 c) February 1972 d) March 1993 e) January 2000. Contoured 5.0 from -17.5 to 15.0 W m^{-2}.

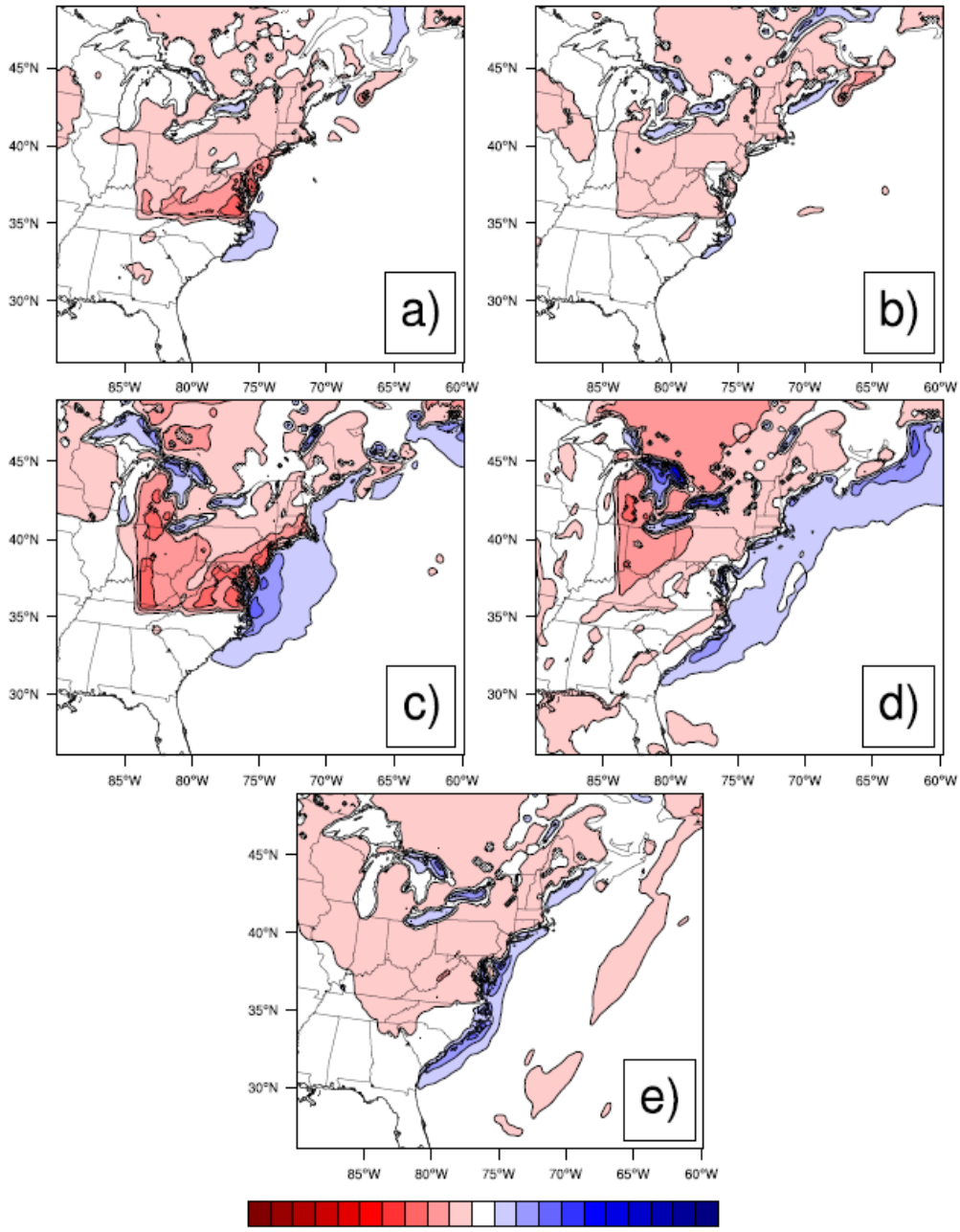

Figure 3.8.6: Average difference in upward sensible heat flux averaged over storm duration and smoothed using 9 point average. a) February 1969 b) December 1969 c) February 1972 d) March 1993 e) January 2000. Contoured by 35.0 from -320.0 to 330.0 W m^{-2}.

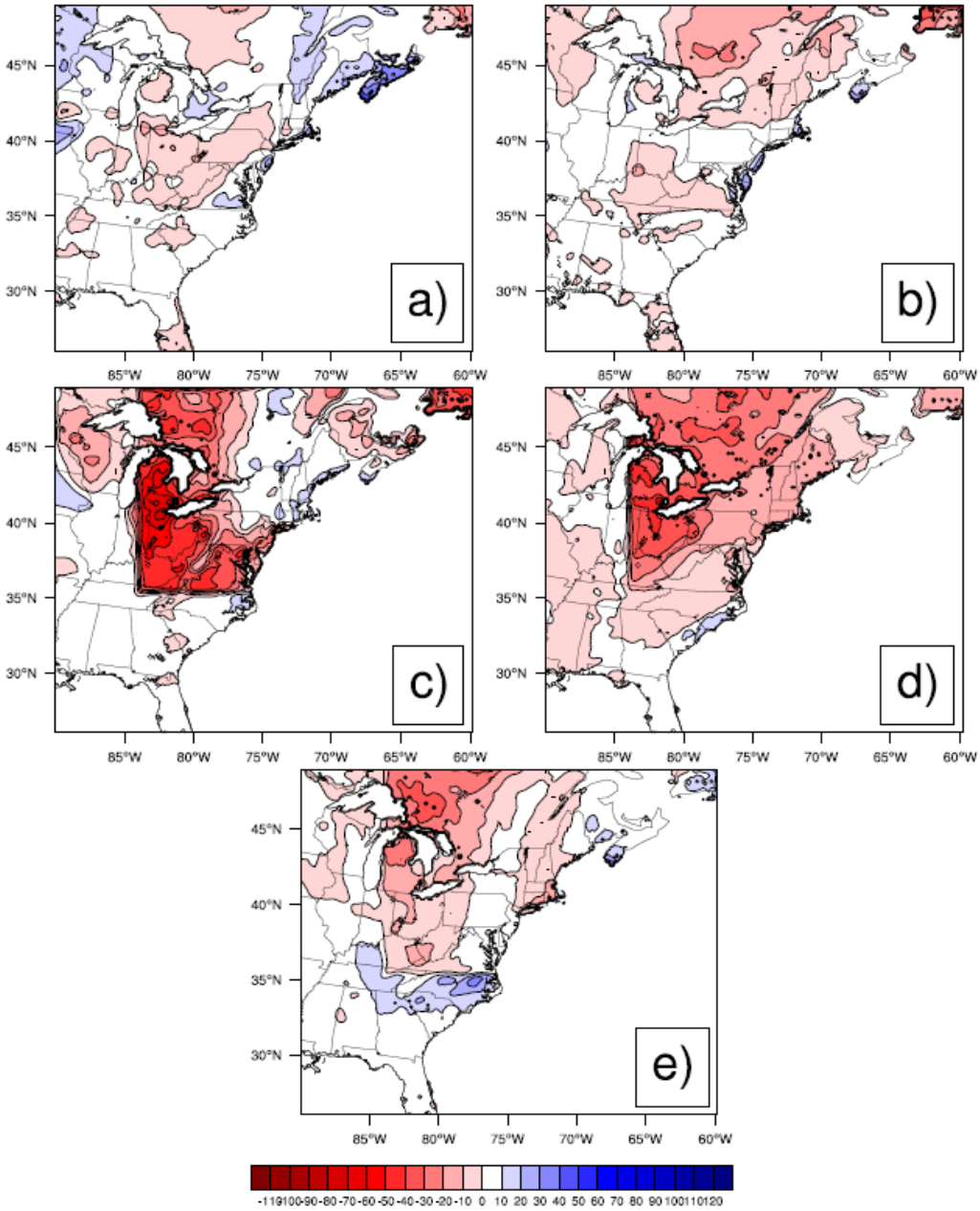

Figure 3.8.7: Average difference in ground heat flux averaged smoothed using 9 point average over the storm duration. a) February 1969 b) December 1969 c) February 1972 d) March 1993 e) January 2000. Contoured from -110.0 to 120.0 by 10.0 W m^{-2}.

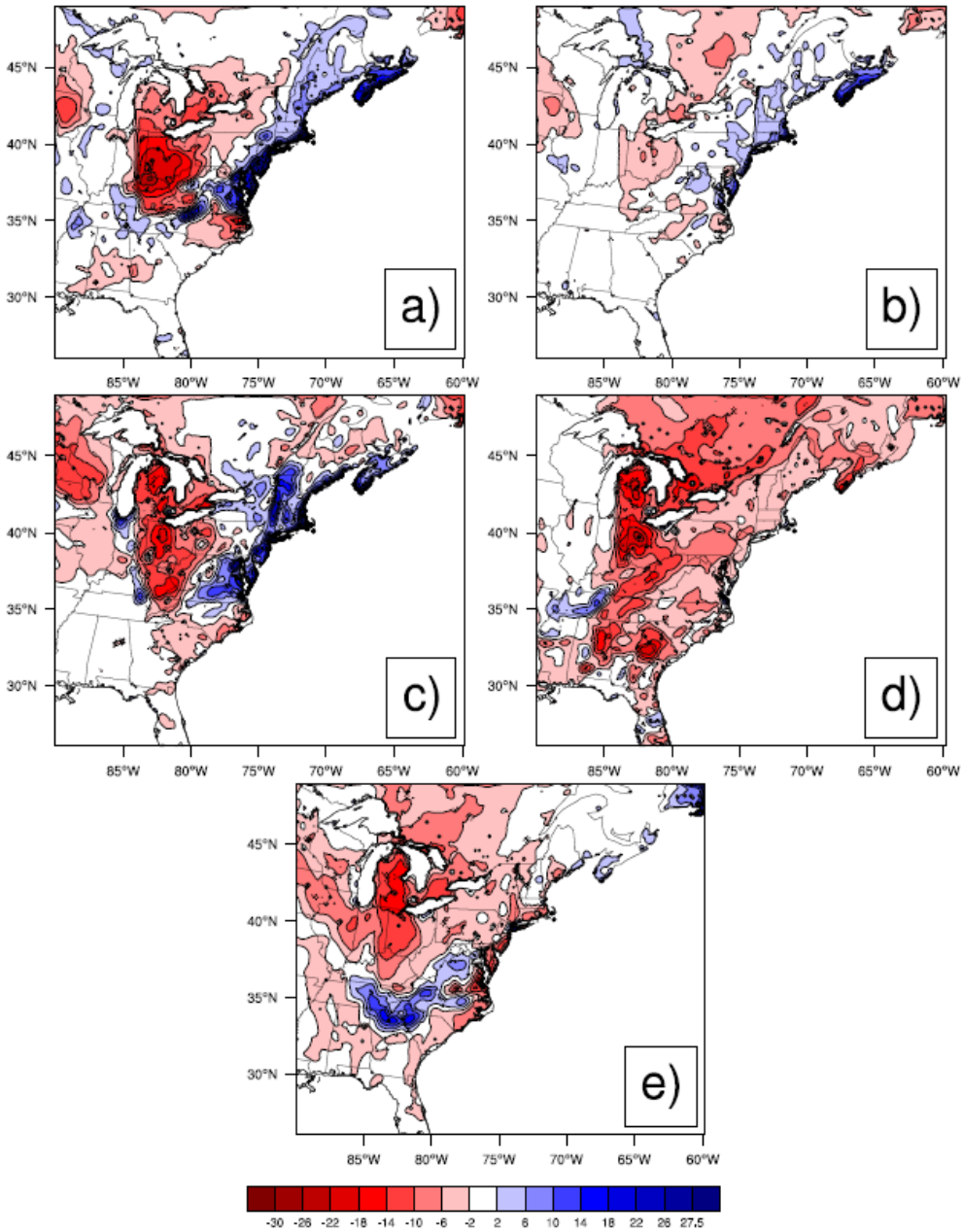

Figure 3.8.8: Differences in upward surface latent heat flux averaged over storm duration smoothed using 9 point average with a landmask. a) February 1969 b) December 1969 c) February 1972 d) March 1993 e) January 2000. Contoured from -30.0 to 27.5 by 4.0 W m^{-2}.

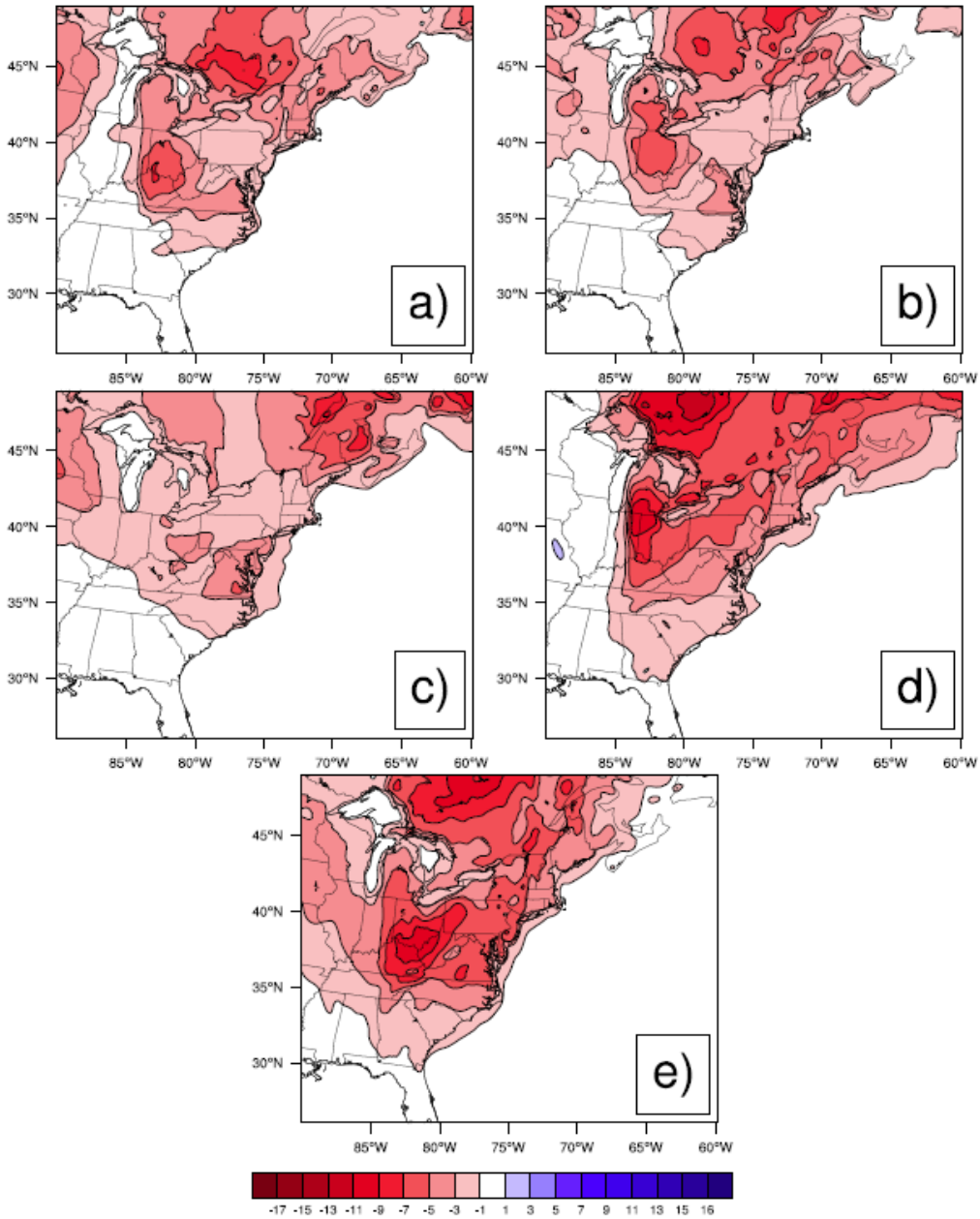

Figure 3.8.9: Average two-meter temperature differences smoothed using a 9 point average over storm duration. a) February 1969 b) December 1969 c) February 1972 d) March 1993 e) January 2000. Contours by 2.0 from -17.0 to 16.0°C.

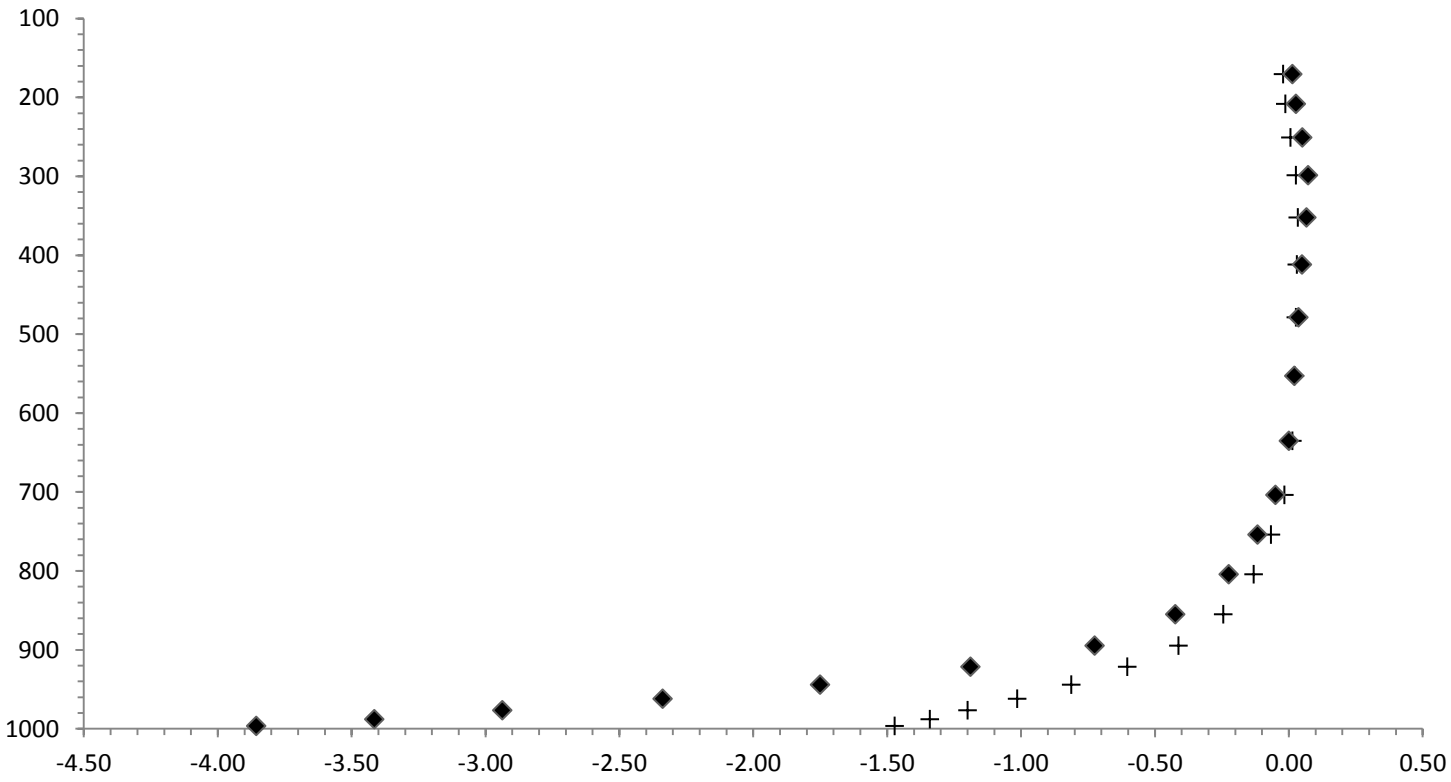

Figure 3.8.10: Average temperature difference of all cases over storm duration and height (η). Average differences over the inner domain are cross hatches and over the northeast are diamonds.

Chapter 4

INDIRECT EFFECTS

4.1 Pressure

4.1.1 Sea level pressure

The average sea-level pressure in the snowpack simulations is 0.9 mb higher than the average sea-level pressure in the snow-free simulation (Table 4.1.1). The higher average sea-level pressure in the snowpack simulations are spatially homogenous and temporally consistent over the Northeast (Figure 4.6.1). The only exceptions to higher pressure in the snowpack simulation occur when the central low pressures of both storms are near land.

The increase in sea-level pressure of the snowpack simulation ranges from 0.3 mb to 1.6 mb (Table 4.1.1). The magnitude of the average sea level pressure increase in the snowpack simulation decreases with height (Table 4.1.2); therefore the pressure increase in the snowpack simulation is a low-level effect. The higher pressure in the snowpack simulations correlates with the lower temperatures in the snowpack simulation, cooling leads to denser, sinking air.

4.1.2 Central low pressure

In all cases except the January 2000 case, the case-averaged hourly central low pressure is greater in the snowpack simulations than in the snow-free simulations. The

average increase in central low pressure of the snowpack simulation is 0.6 mb over all the cases and is 1.0 mb if the January 2000 case is excluded (Table 4.1.3).

The snowpack simulation of the March 1993 case has the largest increase in central low pressure. The December 1969 case has the smallest increase in central low pressure for the snowpack simulation and is only one-sixth the size of the second smallest increase.

The central low pressure differences ranged from -3.4 to 3.9 mb (Table 4.1.3); indicating that the central low pressure is not always greater in a snowpack simulation. The average increase in central low pressure in the snowpack simulation indicates that the nor'easter in the snowpack simulation is typically, but not always, weaker. The central low pressure may be weaker in the snowpack simulation because of the increased stability at the surface due to a decrease in temperature and a decrease in moisture.

Table 4.1.1: The Northeast sea level pressure averaged over storm duration (mb) for the snowpack and snow-free simulations of the 8-10 February 1969, 25-28 December 1969, 18-20 February 1972, 12-14 March 1993, and, 24-26 January 2000.

	Snowpack				Snow-free			
	Average	Minimum	Maximum	Standard Deviation	Average	Minimum	Maximum	Standard Deviation
Feb-69	1015.2	981.2	1034.4	5.5	1014.2	980.4	1033.2	5.5
Dec-69	1018.6	982.0	1036.9	7.7	1018.3	983.0	1035.5	7.5
Feb-72	1009.1	971.9	1036.2	13.5	1008.0	971.0	1034.8	13.4
Mar-93	1012.6	962.4	1030.6	13.4	1011.0	960.1	1028.5	12.9
Jan-00	1018.9	993.8	1032.6	5.2	1018.1	994.8	1031.6	4.8
Average	1014.9	978.3	1034.1	9.0	1013.9	977.9	1032.7	8.8

	Difference			
	Average	Maximum Negative	Maximum Positive	Standard deviation
Feb-69	1.0	-5.0	5.1	0.5
Dec-69	0.3	-4.1	3.6	0.4
Feb-72	1.1	-5.9	9.0	1.0
Mar-93	1.6	-8.5	9.3	1.0
Jan-00	0.8	-4.5	3.4	0.8
Average	1.0	-5.6	6.1	0.7

Table 4.1.2: Pressure differences at given heights, averaged over the northeast landmass for storm duration for the snowpack and snow-free simulations of the 8-10 February 1969, 25-28 December 1969, 18-20 February 1972, 12-14 March 1993, and, 24-26 January 2000.

η	997				962			
	Average	Negative Max. Diff.	Positive Max. Diff.	Standard deviation	Average	Negative Max. Diff.	Positive Max. Diff.	Standard deviation
Feb-69	1.0	-5.0	5.1	0.4	0.9	-4.8	4.9	0.4
Dec-69	0.3	-3.9	3.4	0.4	0.3	-9.5	5.3	0.4
Feb-72	1.0	-5.8	8.5	1.0	1.0	-8.2	10.4	1.0
Mar-93	1.6	-8.5	9.4	1.0	1.5	-8.3	8.7	1.0
Jan-00	0.8	-4.5	3.4	0.7	0.8	-8.0	8.1	0.7
Average	0.9	-5.5	5.9	0.7	0.9	-7.8	7.5	0.7

η	922				855			
	Average	Negative Max. Diff.	Positive Max. Diff.	Standard deviation	Average	Negative Max. Diff.	Positive Max. Diff.	Standard deviation
Feb-69	0.9	-4.6	4.7	0.4	0.8	-4.4	4.3	0.4
Dec-69	0.3	-3.7	5.7	0.4	0.3	-2.9	3.8	0.4
Feb-72	1.0	-9.2	11.2	0.9	0.9	-8.2	8.0	0.9
Mar-93	1.5	-8.1	8.9	1.0	1.4	-7.9	8.0	0.9
Jan-00	0.8	-5.7	5.4	0.7	0.7	-4.1	5.5	0.6
Average	0.9	-6.3	7.2	0.7	0.8	-5.5	5.9	0.6

Table 4.1.3: Central low pressure difference averaged over storm duration (the 36 hours following storm initialization around Cape Hatteras) (mb) for the snowpack and snow-free simulations of the 8-10 February 1969, 25-28 December 1969, 18-20 February 1972, 12-14 March 1993, and, 24-26 January 2000.

	Snowpack				Snow-free			
	Average	Minimum	Maximum	Standard Deviation	Average	Minimum	Maximum	Standard Deviation
Feb-69	978.9	973.0	997.8	7.1	977.7	969.9	998.9	7.7
Dec-69	988.3	981.0	1006.8	7.3	988.2	980.8	1006.6	7.3
Feb-72	978.8	968.6	996.0	8.1	978.0	969.6	995.3	7.6
Mar-93	967.4	961.9	984.3	5.7	965.7	959.7	980.5	5.7
Jan-00	999.9	994.2	1006.2	3.6	1000.9	996.5	1006.5	3.1
Average	982.7	975.7	998.3	6.4	982.1	975.3	997.6	6.3

	Difference			
	Average	Minimum	Maximum	Standard Deviation
Feb-69	1.2	-3.2	3.9	1.5
Dec-69	0.1	-1.5	1.7	0.6
Feb-72	0.8	-1.0	3.2	1.0
Mar-93	1.7	-1.4	4.5	1.5
Jan-00	-1.0	-3.4	0.7	1.0
Average	0.6	-2.1	2.8	1.1

4.2 Trajectories

Storm trajectory was found following the central low pressure path. For three of the five cases the trajectories of the snowpack and snow-free simulations are nearly identical. The cases with similar trajectories are the December 1969 case, the March 1993 case, and the January 2000 case (Figures 4.6.2, 4.6.3, 4.6.4, 4.6.5, and 4.6.6). For the March 1993 case the only difference between the trajectory of the snowpack simulation and the snow-free simulation occurs when the central low pressure reaches the Atlantic (between 21000 UTC on the 13th and 0300 UTC on the 14th). At this time the snow-free simulation tracks closer to the coast, moves northeast quicker, and then delays off the coast of Maryland on the 14th at 0300 UTC (Figure 4.6.5). In the January 2000 case, the snowpack simulation tracks slower than the snow-free simulation for the first nine hours and then has rapid movement between 0300 and 0600 UTC; therefore the differences only occur temporally (Figure 4.6.6). There are no significant differences in the December 1969 case (Figure 4.6.3).

The February cases are the only cases that show notable differences in the nor'easter trajectories. The snowpack trajectory of the February 1969 nor'easter is displaced further north on the ninth between 0000 and 0300 UTC as it tracks overland. After the central low pressure contacts the coast at 0900 UTC the snowpack trajectory tracks further on shore until 1800 UTC. After this time, the nor'easter tracks of the snowpack and snow-free simulations resemble each other (Figure 4.6.2).

The trajectories of the February 1972 case start over the Great Lakes with the snowpack simulation tracking further south. On the 19th at 0600 UTC the central low pressure jumps to the Atlantic in the snowpack simulation. Here the February 1972 case has the same pattern as the February 1969 case in that the snowpack simulation

tracks further inland and the snow-free simulation is further off shore until the central low pressure of the snow-free simulation is back on land (Figure 4.6.4).

In summary, in both the February cases when the central low pressures are initially tracking over the Midwest the snow-free simulations tracks further south when the central low pressures are along the coast the snowpack trajectories are further inland and the control trajectories are westward in the Atlantic. Storm trajectories in the Northeast are strongly influenced by topographic effects (Kocin and Uccellini 2004). The trajectories may be smaller between the two simulations for all cases because the trajectory paths are predetermined by constant geography such as the land-ocean baroclinic zone in the shape of the coastlines and cold air damming along the Appalachians. These permanent features all act to narrow the nor'easter path options, which may be one reason the trajectory of the snowpack simulation did not deviate much from the trajectory of the snow-free simulation. Furthermore, the trajectories are dominated by upper-level influences and the snowpack might only significantly alter the lower atmosphere.

4.3 Atmospheric moisture

The average water vapor mixing ratio in the snowpack simulation is less than the snow-free simulation (Table 4.3.1). Like average temperature, the pattern of lower mixing ratio for the snowpack simulation continues but weakens with height (Figure 4.6.12). The trend of lower average mixing ratio for the snowpack simulation spatially breaks down by η 753; therefore like temperature it is a low level effect. By η of 635 (Table 4.3.1) differences of average mixing ratio are negligible. This is the same level where there are no longer temperature differences between simulations (Section 3.7).

Table 4.3.1: Water vapor mixing ratio differences over the Northeast (g kg^{-1}) for the snowpack and snow-free simulations of the 8-10 February 1969, 25-28 December 1969, 18-20 February 1972, 12-14 March 1993, and, 24-26 January 2000.

η	997				885			
	Average	Maximum Negative	Maximum Positive	Standard deviation	Average	Maximum Negative	Maximum Positive	Standard deviation
Feb-69	-0.4	-3.7	2.8	0.3	0.0	-1.8	1.7	0.2
Dec-69	-0.3	-2.9	2.8	0.3	0.0	-1.6	1.7	0.1
Feb-72	-0.3	-3.9	2.0	0.3	-0.1	-3.0	2.4	0.3
Mar-93	-0.3	-6.3	7.3	0.3	-0.2	-4.1	5.5	0.3
Jan-00	-0.3	-2.0	5.4	0.3	-0.1	-3.3	2.8	0.2
Average	-0.3	-3.7	4.0	0.3	-0.1	-2.8	2.8	0.2
η	704				479			
	Average	Maximum Negative	Maximum Positive	Standard deviation	Average	Maximum Negative	Maximum Positive	Standard deviation
Feb-69	0.0	-3.1	3.0	0.2	0.0	-2.0	1.5	0.1
Dec-69	0.0	-2.7	2.6	0.1	0.0	-1.6	1.1	0.1
Feb-72	0.0	-3.5	2.9	0.3	0.0	-1.4	1.2	0.1
Mar-93	0.0	-5.2	6.1	0.3	0.0	-3.2	2.9	0.2
Jan-00	0.0	-3.4	3.7	0.3	0.0	-1.5	2.0	0.1
Average	0.0	-3.6	3.7	0.2	0.0	-1.9	1.7	0.1

4.4 Stability and vertical motion

Potential temperature is a measure of both temperature and moisture. A profile of potential temperature is an indication of static stability. The potential temperatures of individual cases at noon were examined (Figures 4.6.13 and 4.6.14). Noon is the best time to support turbulence and convection. The potential temperature profiles of the snowpack simulations have greater positive slopes. In terms of convective precipitation, the more positive the slope the faster temperature and moisture decrease with height, and it is less likely the air mass will buoyantly rise; therefore increased positive slope means air is less likely to buoyantly rise indicating increased stability and decreased probability of convection and turbulence. The increased static stability of the snowpack simulation agrees with the more stable, cooler, and drier near-surface conditions found in the simulations.

4.5 Precipitation

4.5.1 Total precipitation

The output precipitation values using WRF Single Moment 6 Scheme are liquid convective, liquid non-convective, snow, and an ice-graupel combination. Non-convective precipitation is produced by processes that can be resolved at grid scale and convective precipitation is subgrid-scale. Total precipitation is the sum of the four precipitation types. The average total precipitation is higher for the snowpack simulation (Table 4.5.1).

On average, the total precipitation increases by 2.8%. In the March 1993 case, the average total precipitation increases by 1.1 mm hr^{-1}. The average precipitation gain in the February cases and the December case is approximately half the value of the

March 1993 case. The gain in precipitation of the January 2000 case is minimal and is not even a quarter of the magnitude of the December and February cases (Table 4.5.1).

It is logical that the January 2000 case has the smallest difference in total average precipitation since it tracks mainly over the Atlantic; therefore the storm system is furthest from the forcing of the snowpack compared to the other simulations.

4.5.2 Convective versus non-convective precipitation

The snowpack simulations produce less convective precipitation and more non-convective precipitation (Table 4.5.1); the only exception is the January 2000 case. The January 2000 case has no difference in non-convective precipitation between simulations and has an increase in convective precipitation for the snowpack simulation.

The average decrease in convective precipitation for the snowpack simulation is 0.1 mm hr^{-1} while the average non-convective precipitation increases by almost three times this amount (Table 4.5.1). Excluding the January 2000 case, there is a 2.9 % loss in convective precipitation and 2.4 % gain in non-convective precipitation

The decrease in convective precipitation as a percent of total precipitation was approximately 40%.

4.5.3 Frozen precipitation

There is an increase in the amount of frozen precipitation produced in the snowpack simulations. The average total precipitation gain in the snowpack simulation is 0.4 mm hr^{-1}. The percent gain in hourly domain-averaged snowfall is more than 10% for graupel and almost 20% for snowfall (Tables 4.5.3 and 4.5.5).

Table 4.5.1: Precipitation values for the snowpack and snow-free simulations of the 8-10 February 1969, 25-28 December 1969, 18-20 February 1972, 12-14 March 1993, and, 24-26 January 2000.

	Difference in Convective					Difference in Non-convective				
	Average	Min.	Max.	Standard Deviation	Total	Average	Mini.	Max.	Standard Deviation	Total
Feb-69	-0.4	-17.9	17.0	2.7	-6198.4	0.5	-96.9	64.8	8.3	17182.4
Dec-69	0.0	-14.7	12.8	2.2	-232.5	0.2	-42.6	41.6	4.4	5880.1
Feb-72	-0.1	-27.6	26.4	3.4	-1675.8	0.2	-67.8	76.6	6.1	6100.3
Mar-93	-0.2	-24.0	21.2	2.6	-2825.4	0.6	-123.7	94.0	7.3	19368.8
Jan-00	0.1	-63.2	52.0	9.2	1605.8	0.0	-202.2	157.1	9.0	112.2
Average	-0.1	-29.5	25.9	4.0	-1865.3	0.3	-106.6	86.8	7.0	9728.8

Total Difference

	Average	Mini.	Max.	Standard Deviation	Total
Feb-69	0.6	-94.8	62.5	8.9	21800.4
Dec-69	0.4	-42.5	40.8	5.0	13934.4
Feb-72	0.5	-71.1	72.6	8.0	15313.9
Mar-93	1.1	-106.0	98.1	8.8	39486.3
Jan-00	0.1	-189.4	163.9	11.4	2825.5
Average	0.5	-100.7	87.6	8.4	18672.1

Table 4.5.2: Inner domain-averaged hourly snowfall (mm hr^{-1}) for the snowpack and snow-free simulations of the 8-10 February 1969, 25-28 December 1969, 18-20 February 1972, 12-14 March 1993, and, 24-26 January 2000.

	Snowpack			Snow-free		
	Average	Minimum	Standard Deviation	Average	Minimum	Standard Deviation
Feb-69	1.1	34.5	2.8	0.8	34.7	2.4
Dec-69	2.3	44.6	4.4	2.1	41.9	4.1
Feb-72	2.1	43.0	4.4	1.8	43.1	4.1
Mar-93	3.5	60.3	7.1	2.8	49.7	5.8
Jan-00	1.7	28.3	3.1	1.6	22.7	2.9
Average of Cases	2.1	42.1	4.4	1.8	38.4	3.9

Table 4.5.3: Inner domain-averaged hourly snowfall differences (mm hr^{-1}).

	Difference (Snow - Snow-free)				
	Average	Maximum Negative	Maximum Positive	Standard Deviation	Percent gain/loss
Feb-69	0.3	-9.5	18.6	1.0	32.9
Dec-69	0.2	-12.0	14.1	0.8	11.2
Feb-72	0.3	-13.4	19.1	1.1	18.1
Mar-93	0.7	-10.6	22.9	2.1	23.2
Jan-00	0.2	-10.5	11.0	0.7	11.5
Average of Cases	0.3	-11.2	17.1	1.1	19.4

Table 4.5.4: Inner domain-averaged hourly graupel (mm hr^{-1}) for the snowpack and snow-free simulations of the 8-10 February 1969, 25-28 December 1969, 18-20 February 1972, 12-14 March 1993, and, 24-26 January 2000.

	Snowpack			Snow-free		
	Average	Minimum	Standard Deviation	Average	Minimum	Standard Deviation
Feb-69	0.4	49.4	1.9	0.3	36.9	1.6
Dec-69	1.1	37.3	3.3	1.0	34.5	3.1
Feb-72	0.8	55.8	2.8	0.8	60.9	2.7
Mar-93	2.5	74.1	8.1	2.5	73.0	8.0
Jan-00	0.6	42.4	2.5	0.6	45.7	2.5
Average of Cases	1.1	51.8	3.7	1.0	50.2	3.6

Table 4.5.5: Inner domain-averaged hourly graupel (mm hr^{-1}).

	Difference (Snow - Snow-free)				
	Average	Maximum Negative	Maximum Positive	Standard Deviation	Percent gain/loss
Feb-69	0.1	-13.3	24.1	1.1	34.4
Dec-69	0.1	-10.3	14.5	0.9	7.1
Feb-72	0.1	-15.5	27.0	1.2	7.3
Mar-93	0.0	-32.9	35.8	2.1	1.1
Jan-00	0.0	-8.2	8.6	0.4	6.0
Average of Cases	0.1	-16.0	22.0	1.1	11.2

4.6 Clouds

Cloud cover is computed and therefore responds to changing surface conditions, especially as surface temperatures and moisture input influence CAPE, Convective Available Potential Energy, and MSE, Moist Static Energy. As with precipitation, convective clouds are subgrid scale and non-convective clouds are grid scale.

There was a slight increase in integrated cloud depth but it was not significant. The increase in clouds could be from the increased baroclinicity between ocean and land.

With the exception of the March 1993 case, there is no pattern or typical result in arrangement of integrated cloud-depth differences between the snowpack and snow-free simulations. The March 1993 case on the 14th from 0600 to 1500 UTC has more integrated cloud depth banded from north to south in the snowpack simulation compared to the snow-free simulation followed by lower amounts indicating that the nor'easter snowpack simulation is moving slower. This agrees with the trajectory paths of the central low pressures (Section 4.2).

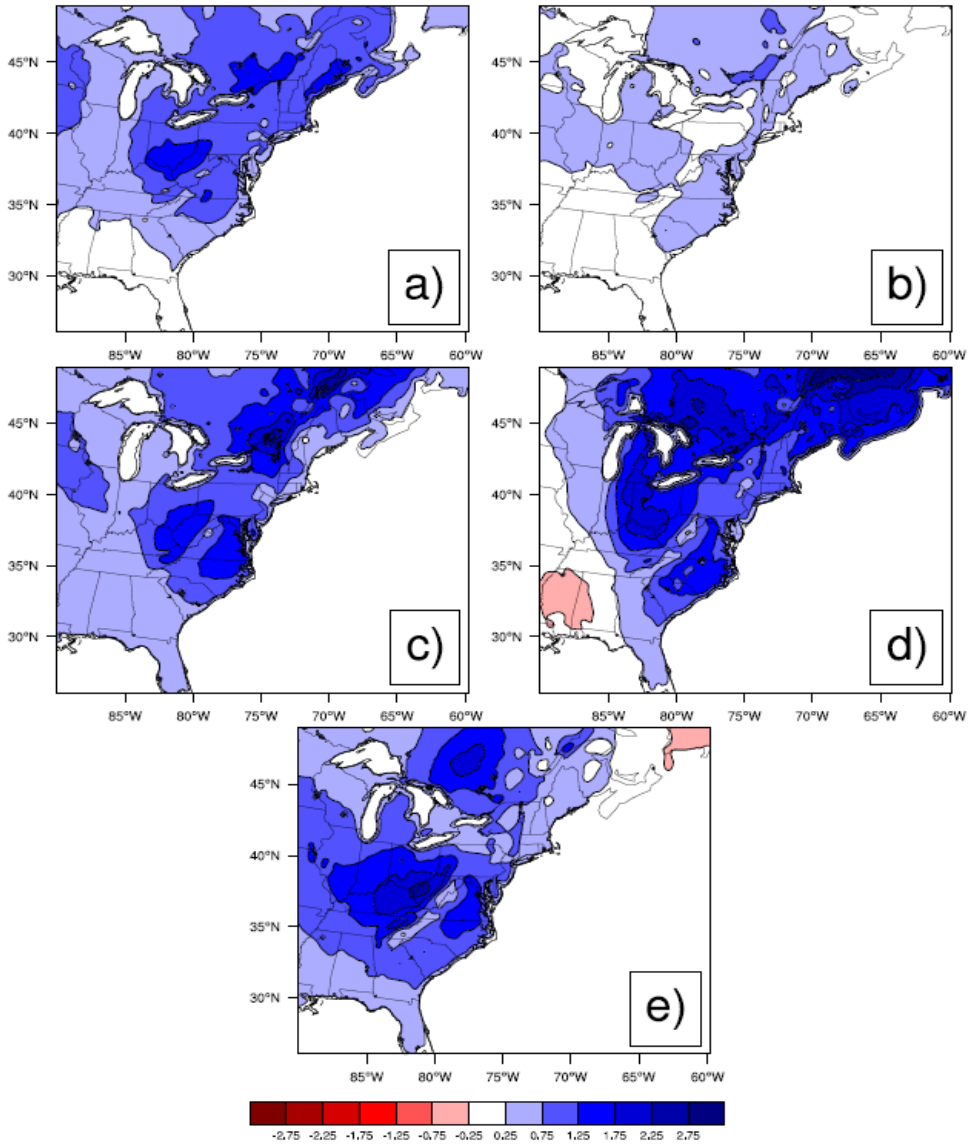

Figure 4.6.1: Average differences in sea level pressure over storm duration smoothed using a 9 point average. a) February 1969 b) December 1969 c) February 1972 d) March 1993 e) January 2000. Contoured from -2.8 to 2.8 by 0.5 mb.

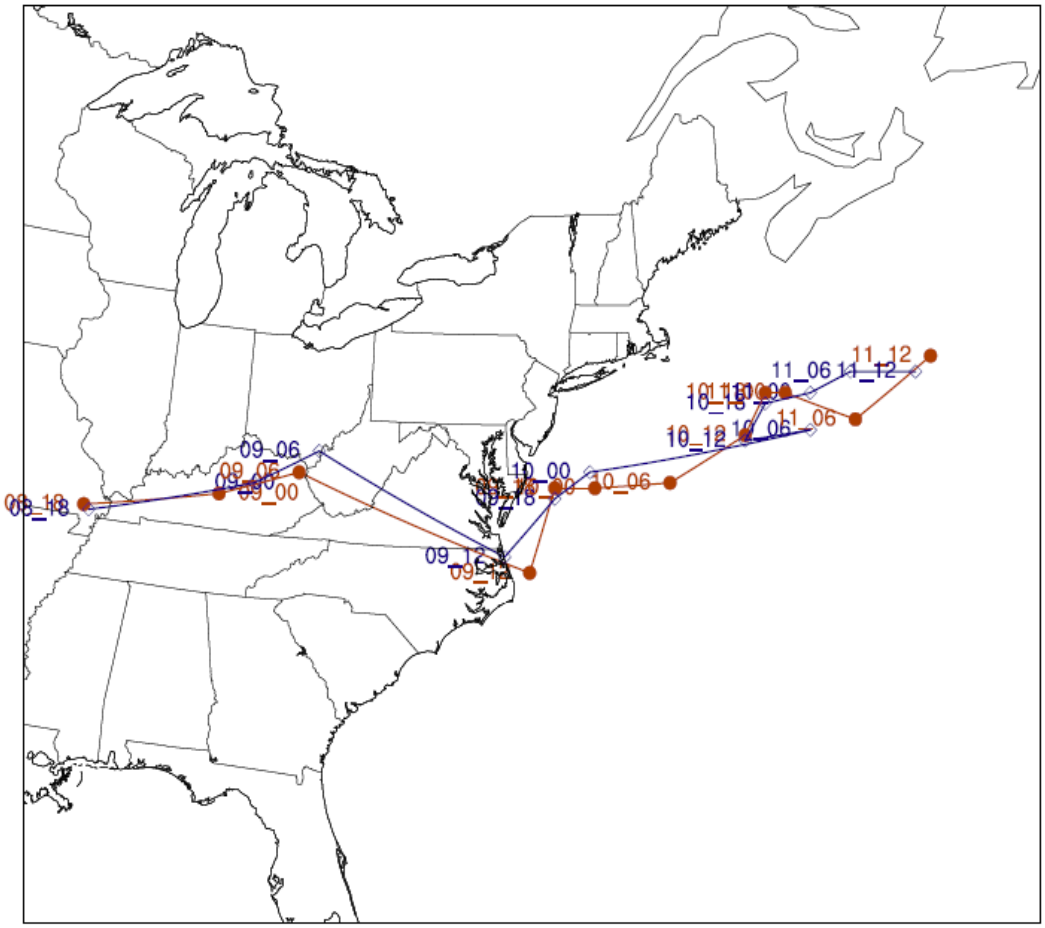

Figure 4.6.2: February 8-11, 1969 modeled storm trajectory following the path of the central low pressure. Red represents the snow-free simulation and blue the snow simulation.

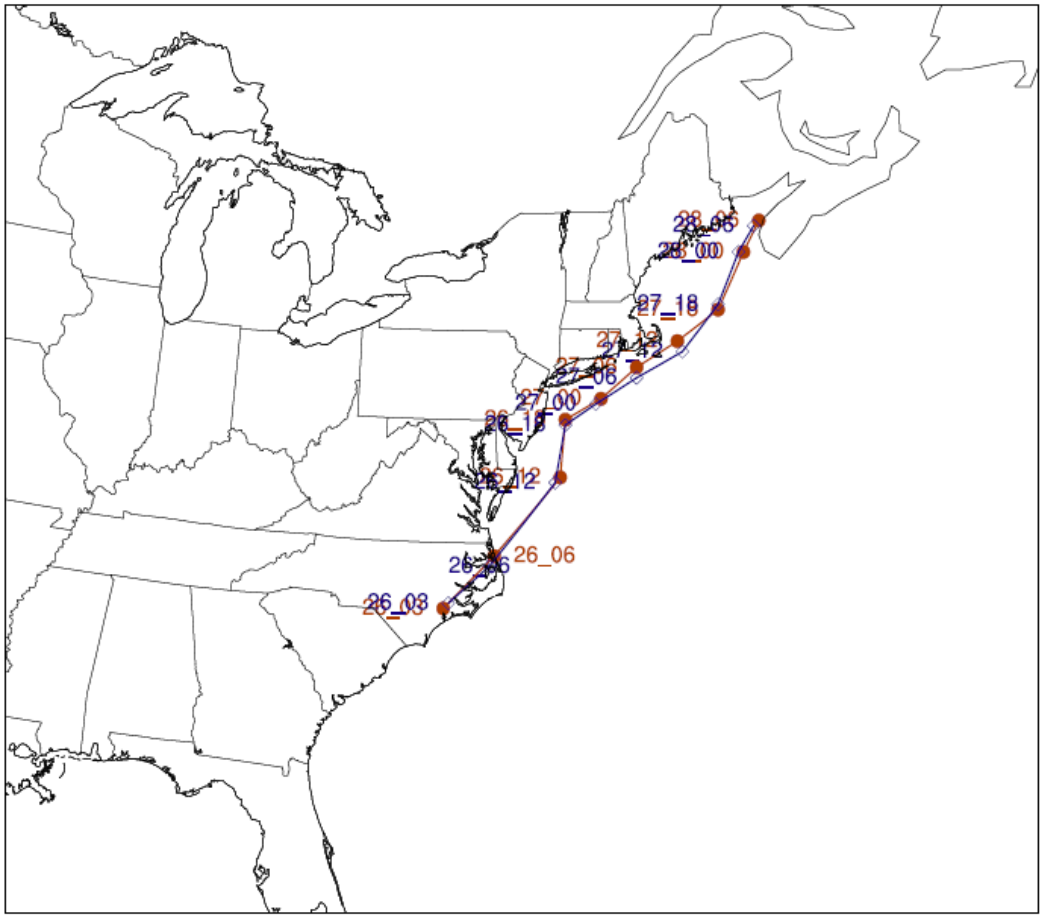

Figure 4.6.3: December 26-28, 1969 modeled storm trajectory following the path of the central low pressure. Red represents the snow-free simulation and blue the snow simulation.

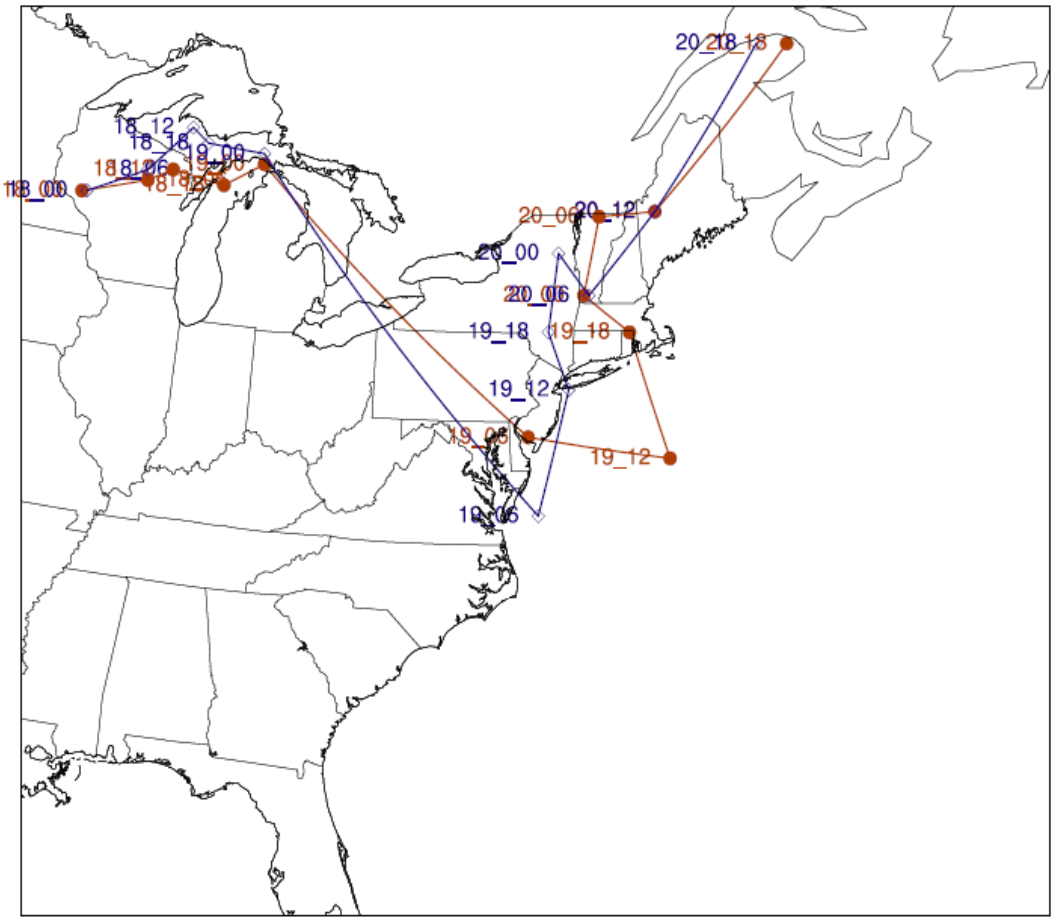

Figure 4.6.4: February 18-20, 1972 modeled storm trajectory following the path of the central low pressure. Red represents the snow-free simulation and blue the snow simulation.

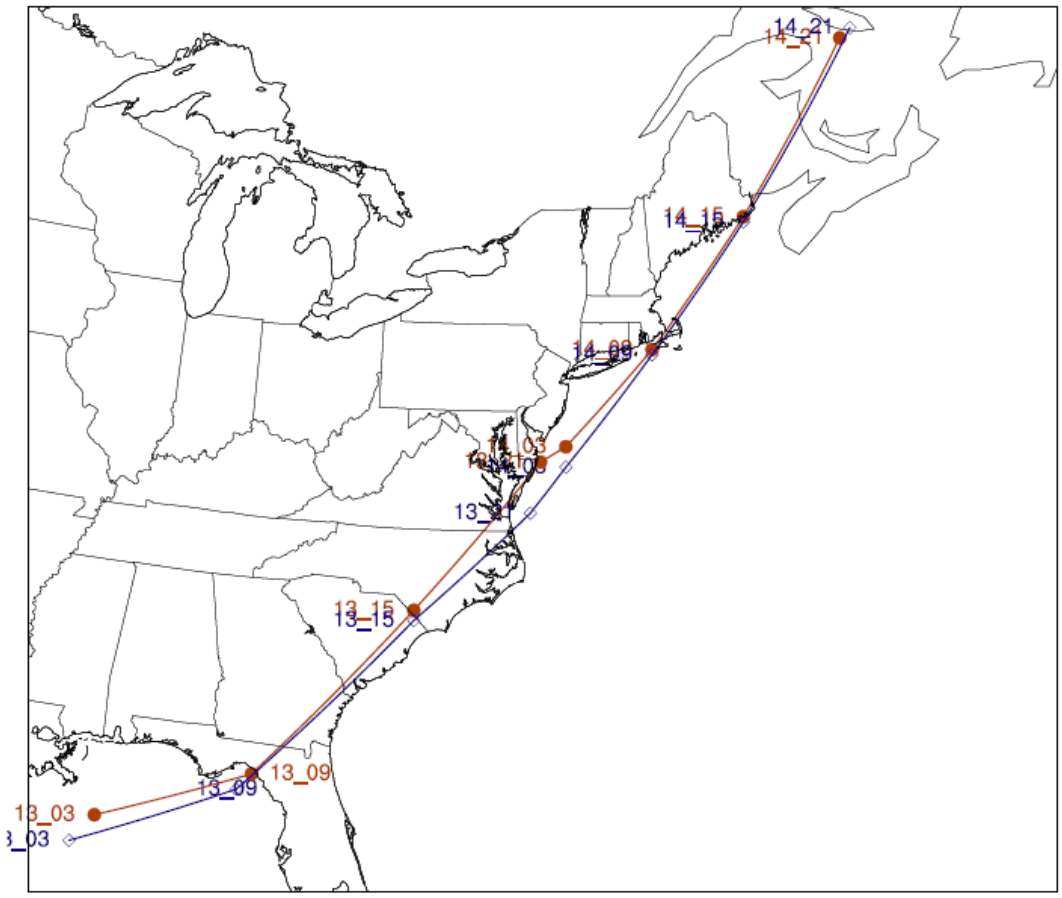

Figure 4.6.5: March 13-14, 1993 modeled storm trajectory following the path of the central low pressure. Red represents the snow-free simulation and blue the snow simulation.

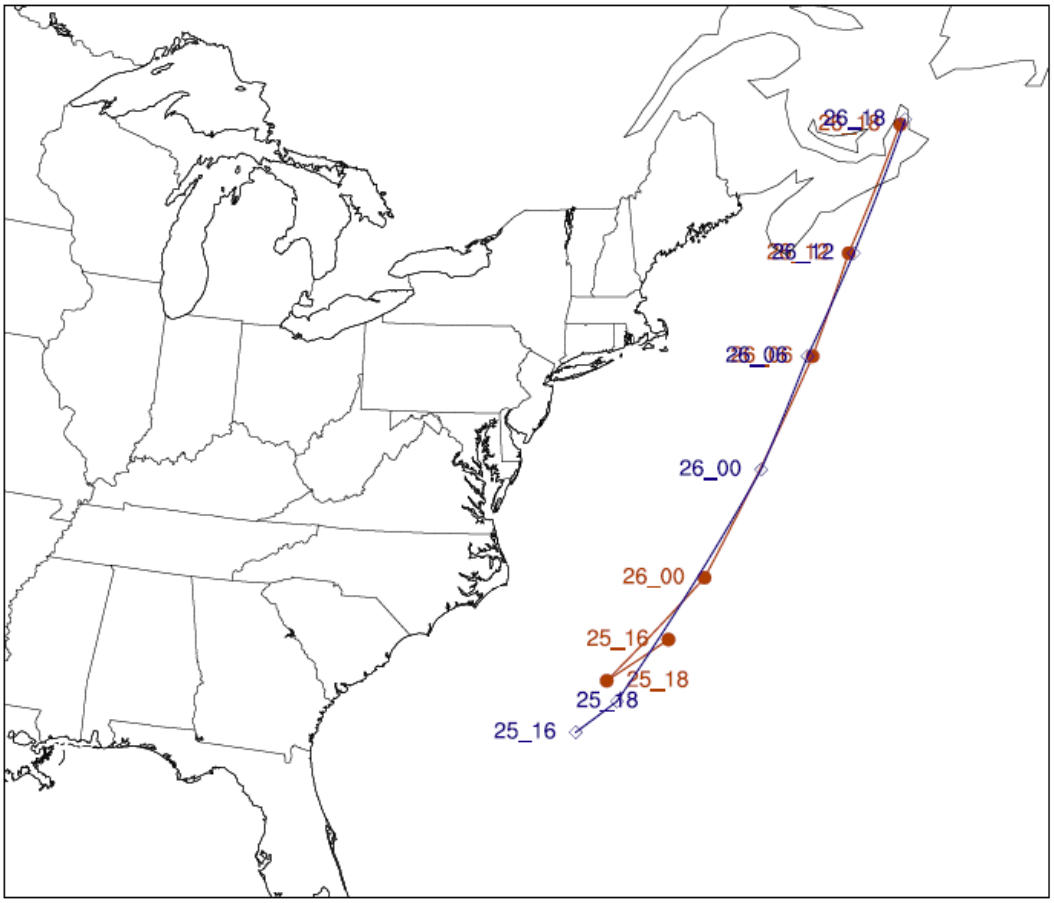

Figure 4.6.6: January 25-26, 2000 modeled storm trajectory following the path of the central low pressure. Red represents the snow-free simulation and blue the snow simulation.

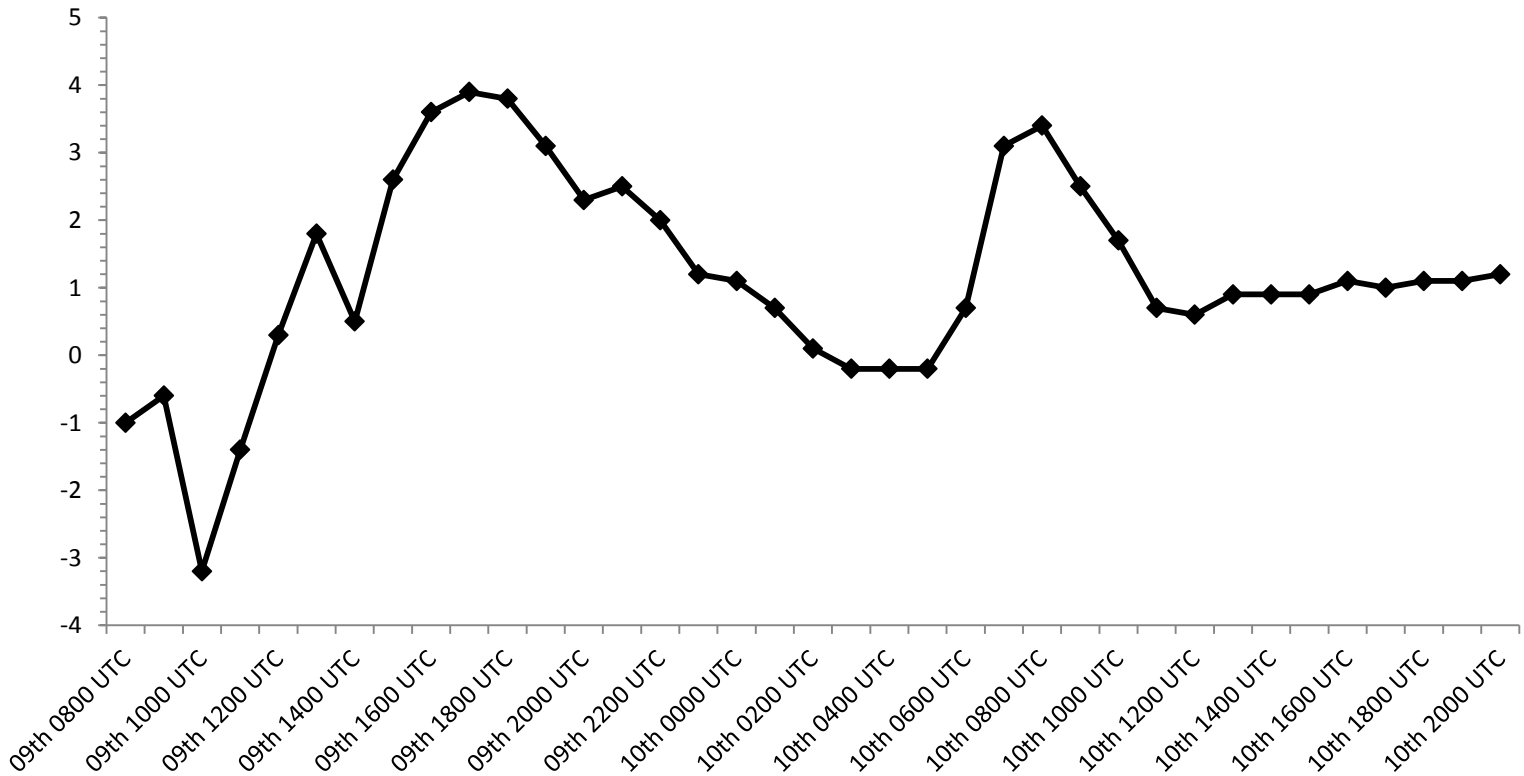

Figure 4.6.7: February 1969 average central sea level pressure rate change (mb hr^{-1}).

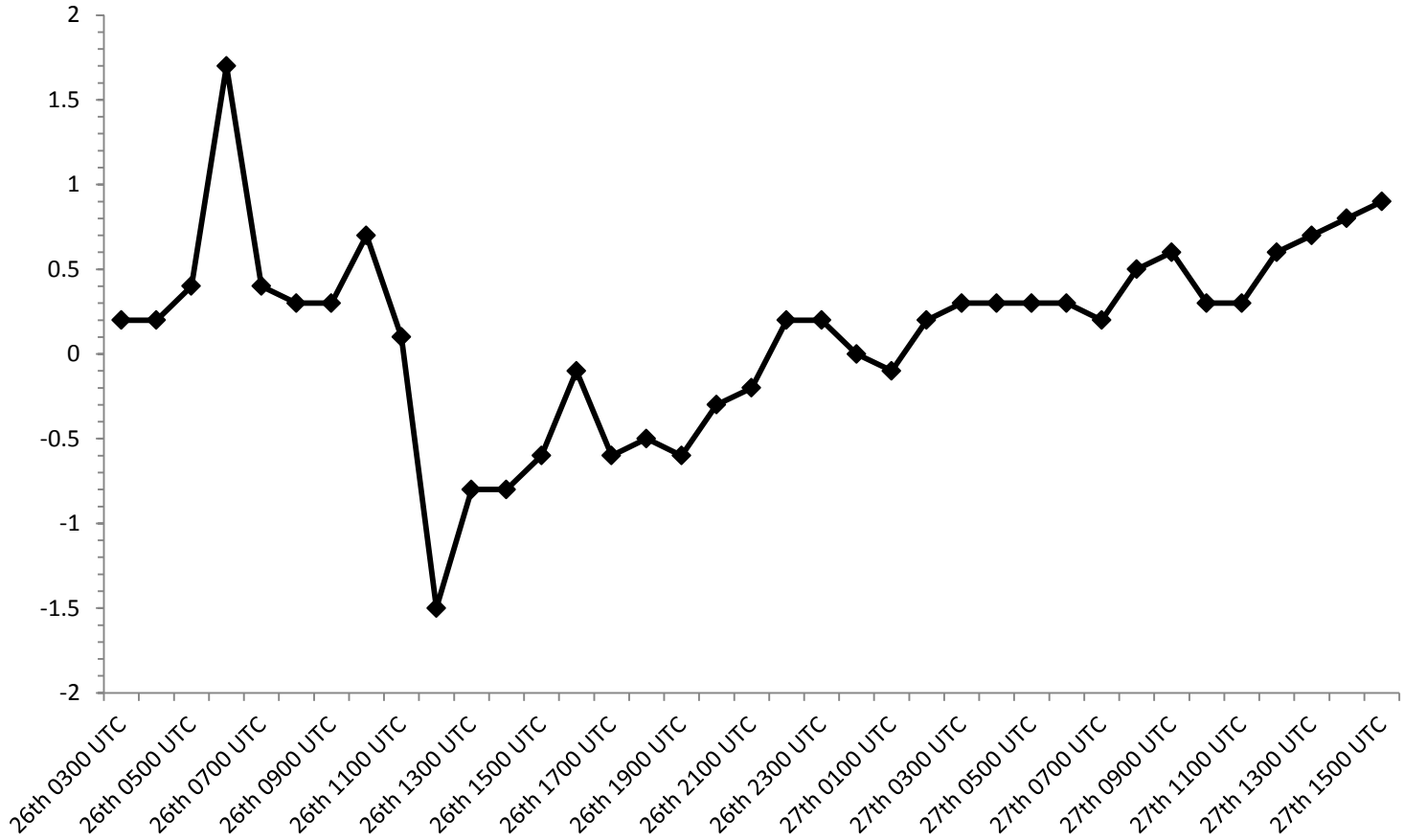

Figure 4.6.8: December 1969 average central sea level pressure rate change (mb hr^{-1}).

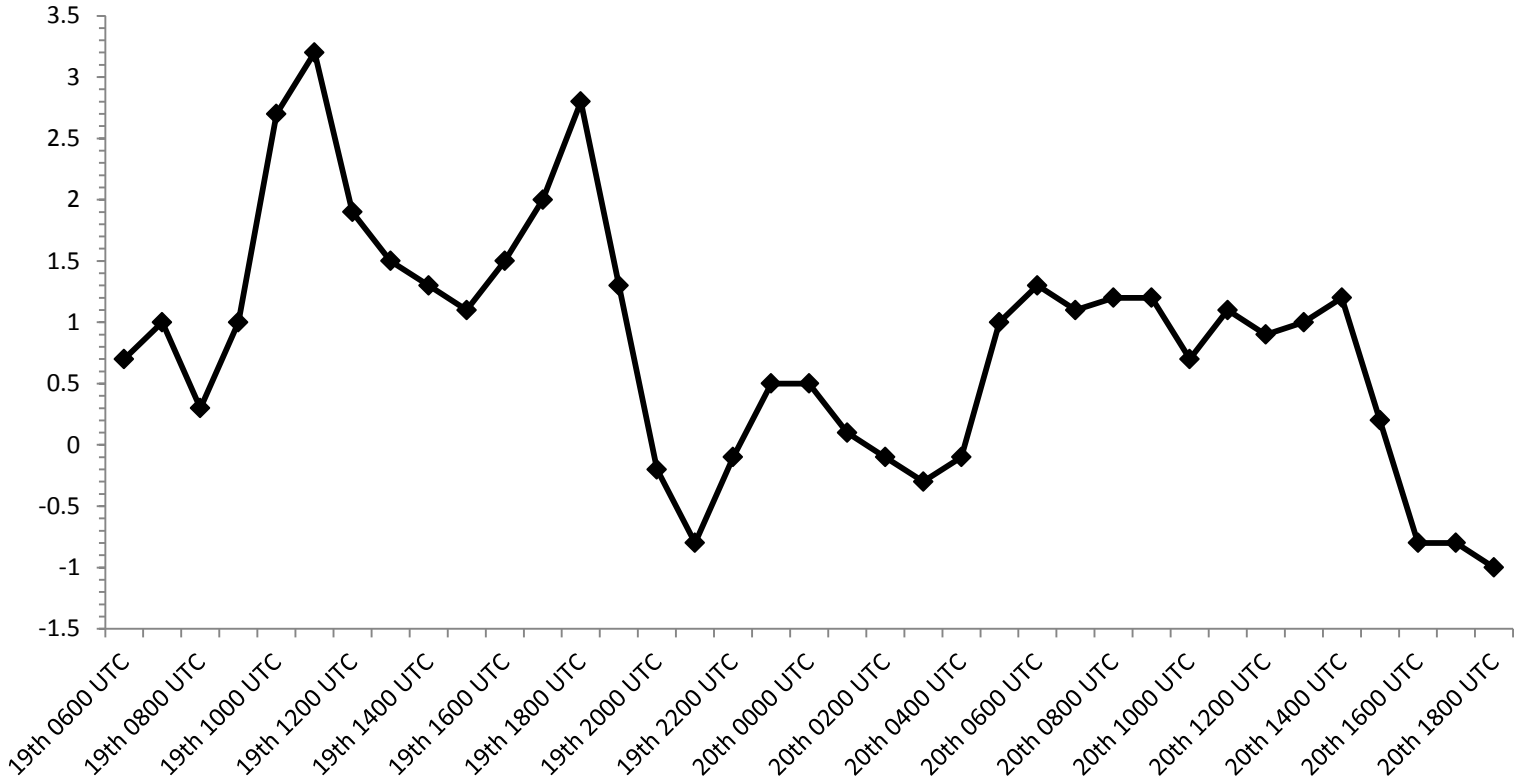

Figure 4.6.9: February 1972 average central sea level pressure rate change (mb hr^{-1}).

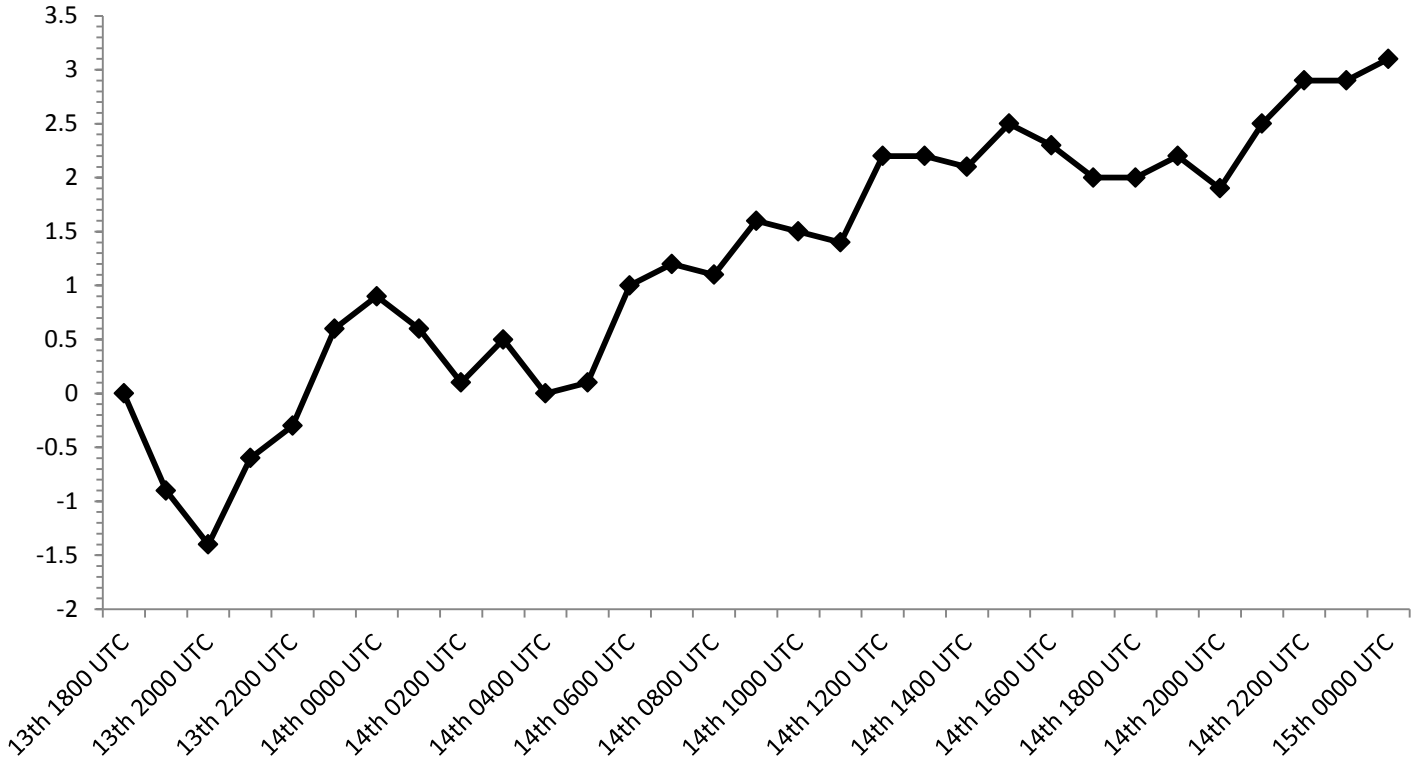

Figure 4.6.10: March 1993 average central sea level pressure rate change (mb hr^{-1}).

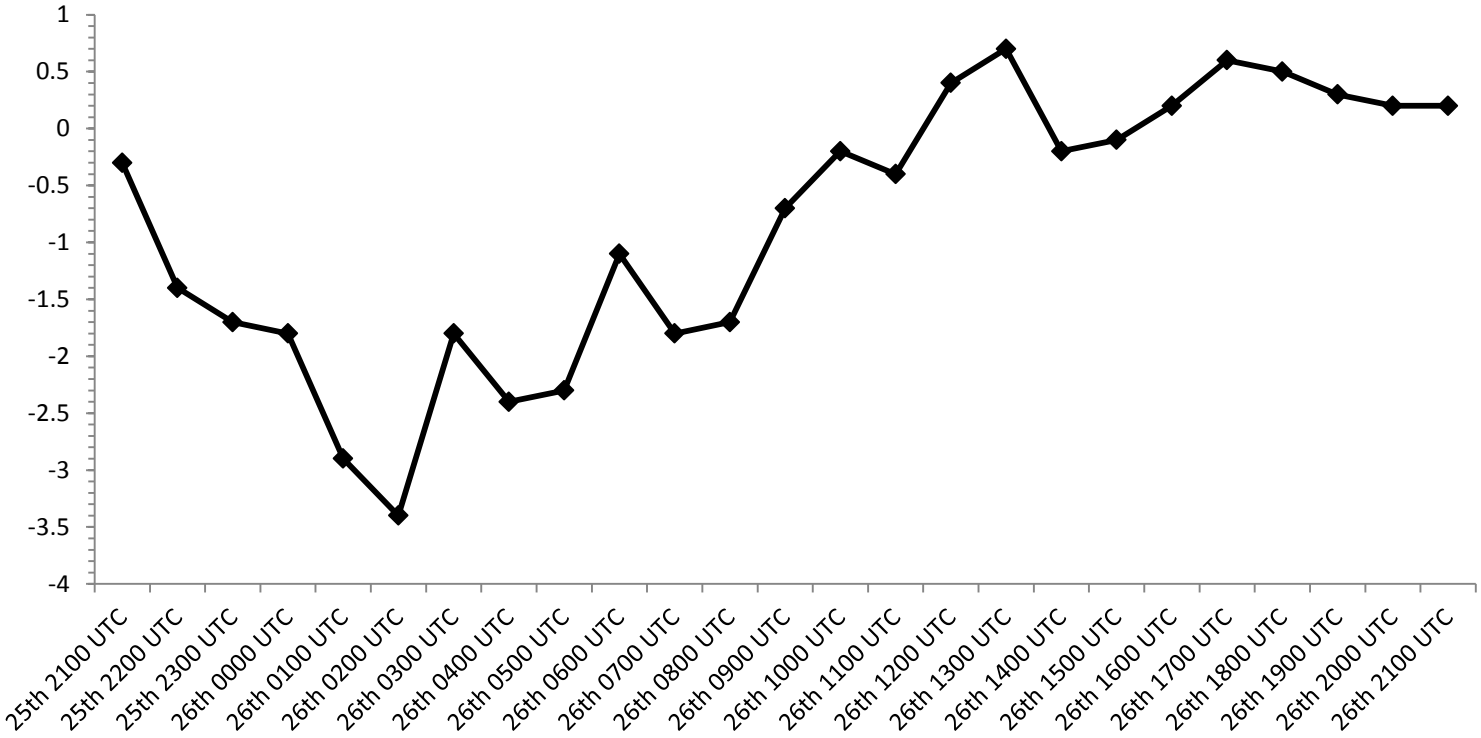

Figure 4.6.11: January 2000 average central sea level pressure rate change (mb hr^{-1}).

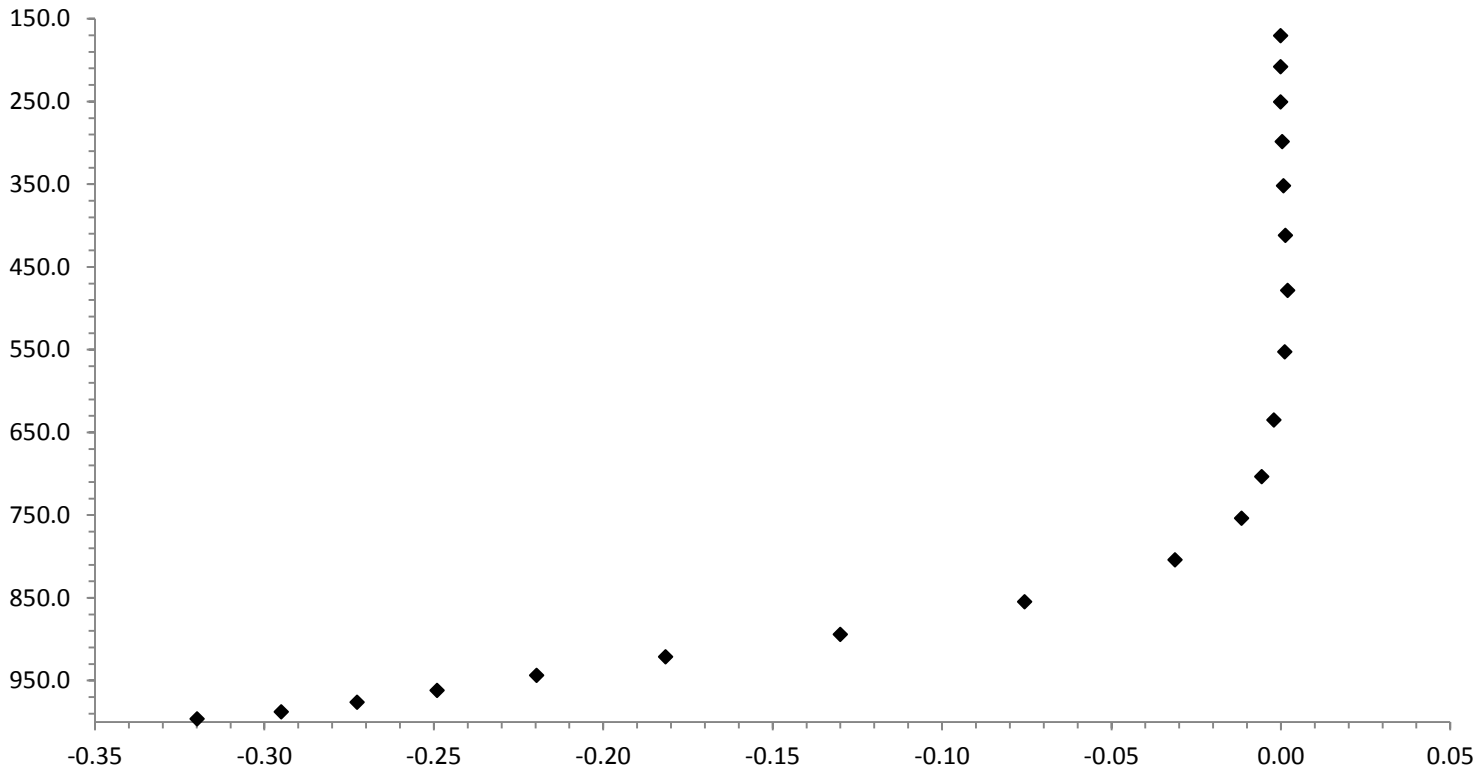

Figure 4.6.12: Height (η*1000) verse change in water vapor mixing ratio averaged over storm duration over the Northeast United States (g kg^{-1}).

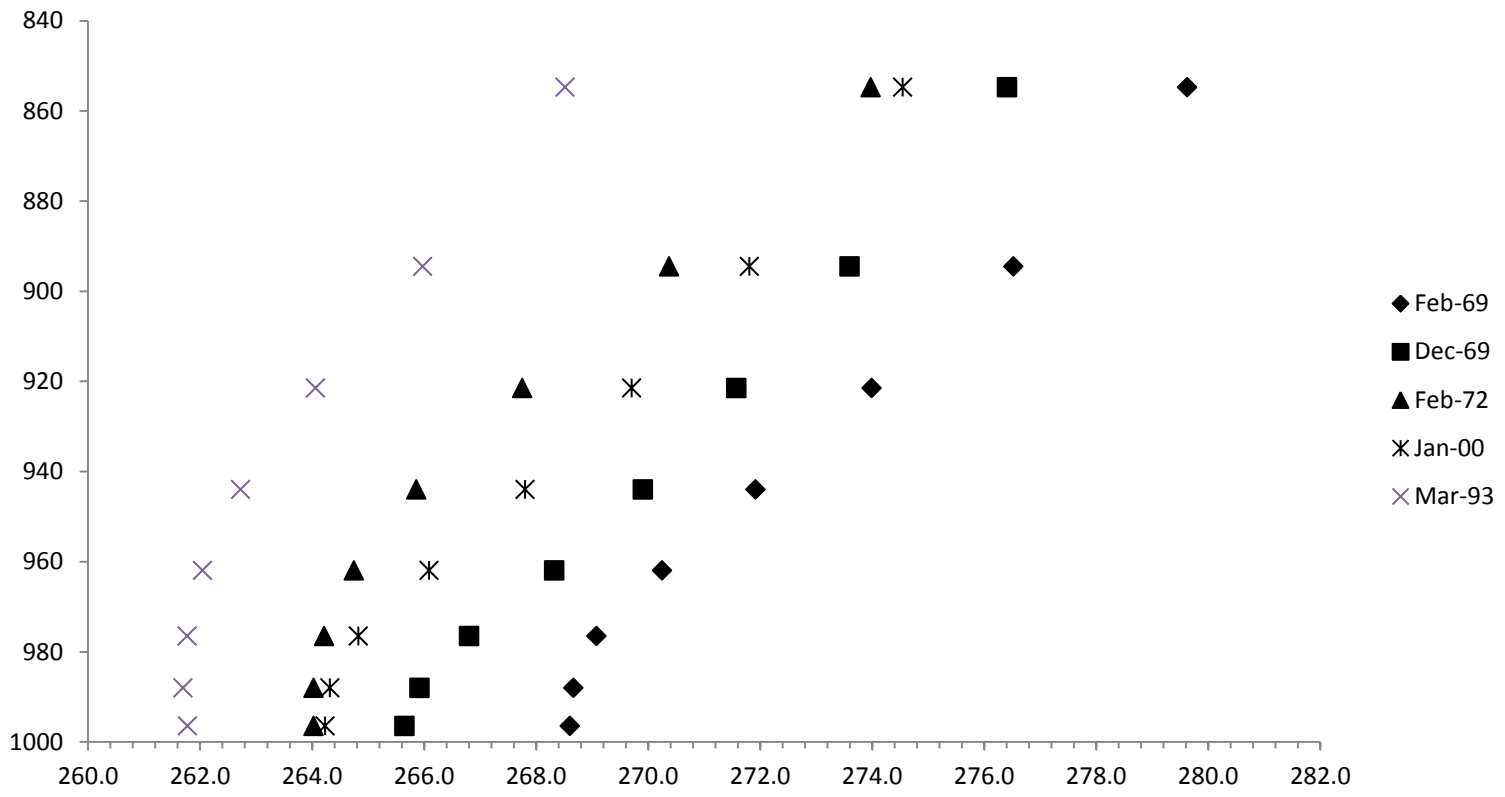

Figure 4.6.13: Case average afternoon snowpack potential temperature (Kelvin) over the Northeast United States verse height (η).

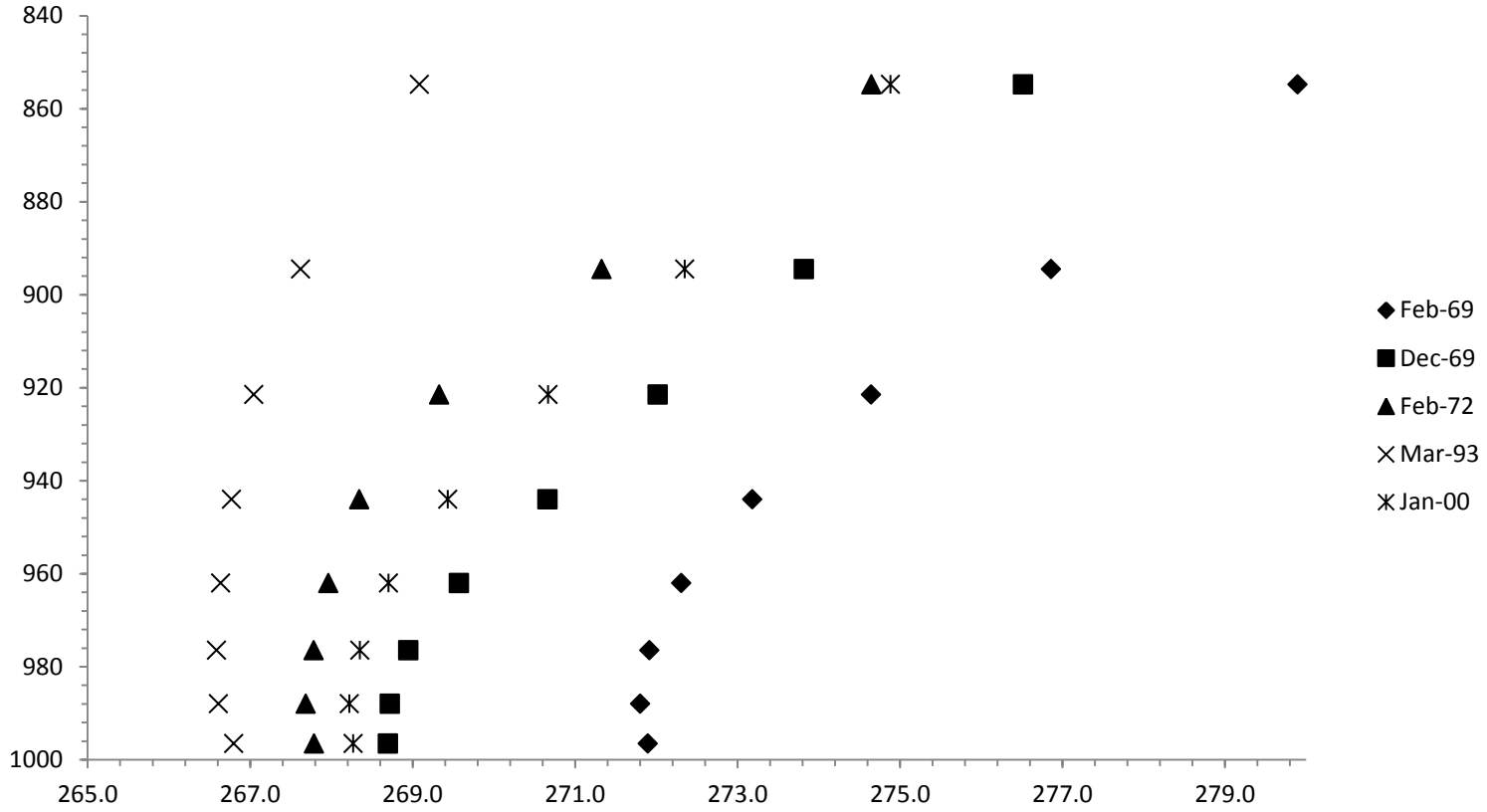

Figure 4.6.14: Case afternoon average snow-free potential temperature (Kelvin) over the Northeast United States verse height (η).

Chapter 5

DISCUSSION

5.1 Net energy fluxes

The energy fluxes reported in Chapter 3 are of similar extent and magnitude to the values reported in other snowpack studies (Baker et al., 1992; Cohen and Rind, 1991; Ellis and Leathers, 1998; Ellis and Leathers, 1999) (Table 5.7.1 and 5.7.2). The snowpack results in a strong reduction in the surface energy which creates lower atmospheric changes that include decreased temperature and moisture, and increased pressure and stability.

5.2 Temperature

The decrease in the average surface temperature of the snowpack simulation reported in section 3.7 is within the range of those reported in other simulations and observational studies (Ellis and Leathers 1998; Walsh et al. 1982; Baker et al. 1992).

Following Cohen and Rind (1991), an approximation of the average temperature difference that would result from the average albedo difference is calculated using the Stefan-Boltzmann Law equated to absorbed solar radiation, $\sigma*T^4 = (1-\alpha)*S_0$. The result is a temperature difference of -7.9° C. Similar to Cohen and Rind (1991), the resultant temperature change is approximately twice as large the observed temperature difference. Since the observed is half of what the temperature change would be just due to the reduction of absorbed solar radiation it indicates that there exist other forces mitigating the albedo effects.

The confinement of the temperature differences to the lower atmosphere or the reduction of atmospheric temperature differences with height described in section 3.7 has been reported in other studies (Cohen and Rind 1991, Namias 1985, Walland and Simmonds 1996, Walsh et al. 1982). Walsh et al. (1982) found that at a sigma-level of 0.93 the maximum temperature differences is one-third the surface temperature difference, and at a sigma-level of 0.81 it is less than one-tenth of the surface temperature difference. Walland and Simmonds (1996) reported temperature differences at 850 mb had similar spatial extent to the near surface differences but with a smaller magnitude, and by 500 mb the temperature differences were smaller in both the magnitude and extent. Namias (1985) observed that snow cover in the Eastern United States only decreased atmospheric temperatures below 850 mb. The decreasing temperature differences with height indicate that the snowcover only directly affects lower atmospheric conditions.

5.3 Pressure

The higher pressure of the snowpack simulation is congruent with its cooler near surface temperatures and is in agreement with other snowpack studies (Spar 1973, Walsh and Ross 1988, Walsh et al. 1982).

The average increase in the central low pressure is 0.6 mb indicating that the nor'easters in the snowpack simulations are weaker. Similar to this study, Ross and Walsh (1986) found a weaker intensification of winter storms in North America for a snowpack between 85 and 70° W.

The changes in the central low pressure reported in section 4.1.2 were not strong compared to the changes in central low pressure for wintertime cyclones in the Midwest and the changes in the Midwest were considered weak, and inconsistent

(Elguindi et al 2005). The comparison of the results from the East Coast and Midwest parallels a statistical study of snow cover occurring in the East and Midwest United States that found as snow cover extent increased from the Mississippi River to 100° W the atmospheric pressure also increased but the positive relationship was only significant in the Midwest (Trapasso and Simpson 1988). It was hypothesized that the relationship was not significant on the East Coast because of both topographic effects (i.e., the Appalachians) and oceanic and lake effects (Trapasso and Simpson 1988).

5.4 Moisture and stability

Like temperature and pressure changes, moisture changes were greatest near the surface. The snowpack simulation displayed drier atmospheric conditions, seen in the reduction of the average water vapor mixing ratio (Section 4.3).

Similar to other snowpack studies, the snowcover ultimately acted to increase static stability; indicated by the more positive potential temperature profiles in the snowpack simulations (Section 4.4) (Cohen and Rind 1991; Elguindi et al., 2005).

5.5 Trajectory and baroclinicity

While this study did not find a notable relationship between storm trajectory and snowcover, Ross and Walsh (1986) found storm tracks for snowpacks tend to increase their motion parallel to the snow cover line and Trappaso and Simpson (1988) found increased snow cover extent displaces storm tracks to the south.

The results reported in section 4.2 are more similar to Elguindi et al. (2005). Elguindi et al. (2005) found that snowcover only changed the trajectory in two of eight simulations and changes did not display any meaningful patterns. Section 4.2 reports

only two of the five the simulations had notable changes to their storm tracks and the changes were not significant.

It is logical that the storm tracks do not change on the East coast because storm tracks generally follow the baroclinic zone. The land-ocean contrast in the northeast provides a well-defined baroclinic zone resulting in nor'easters following similar paths up the Atlantic coast. To change the trajectories would require a substantial shift in the baroclinic zone and the snowpack does not provide a perturbation of this magnitude.

5.6 Precipitation

The total precipitation increased by 2.8%. The total increase in precipitation was from an increase in the non-convective and frozen precipitation while the convective precipitation decreased. Namias (1985) and Elguindi et al. (2005) found decreased precipitation during snow cover periods, but similar to this study Elguindi et al. (2005) found that nearly all of the convective precipitation does not develop in the snowpack simulation due to increased stability and decreased convergence (Elguindi et al. 2005).

The loss in convective precipitation in the snowpack simulations may be due to the overall increase in stability resulting from decreased surface temperatures. The possible increased stability could also be from a decrease in frontal strength. The decreased frontal strength is likely to occur because the gradient across fronts is lower as moisture or temperature changes become more similar.

5.7 Conclusion

The modifications to the nor'easter due to the lower atmospheric surface flux changes were an increase in the central low pressure and total precipitation; with a

decrease in convective precipitation and an increase in frozen and non-convective precipitation. The storm tracks were more or less identical between simulations.

The resultant changes in the nor'easters are much weaker than changes seen in wintertime cyclones in the Midwest (Elguindi et al., 2005). In the Northeast there is a predefined baroclinic zone created by the land/ocean contrast that does not exist in the Midwest; therefore creating a snowpack in the Midwest creates a baroclinic zone by the snow/land thermal contrast resulting in a greater influence from snow on cyclones. Not only is the land/ocean contrast on the East Coast a stronger forcing than the snow/snow-free contrast in the Midwest but the snowpack on the East Coast acts to enhance the land/ocean contrast with even colder land adjacent to the warm ocean.

The energy flux changes resulting from the snowpack driving lower atmospheric changes were not strong enough to significantly alter the modeled nor'easters; indicating that the upper-level dynamics and existing geographic controls (cold air damming, land/ocean contrast, etc.) that create and drive a cyclone are too strong to be considerably altered. Since the strong and idealized forcing of a 50 cm snowpack covering the Northeast United States only results in minor changes to nor'easters, it is unlikely that a realistic snow cover in the Northeast would have any significant influence on a developing wintertime nor'easter.

Table 5.7.1: Reported energy fluxes from snowpack studies.

	McGowan 2012			Baker et al. 1992			Cohen and Rind 1991		
	Snow	Free	Difference	Snow	Free	Difference	Maximum	Minimum	Difference
Albedo	0.30	0.60	0.30	0.80	0.20	0.60			
Downward shortwave	74.6	72.0	2.6	99.8	105.4	5.6			
Upward shortwave	-48.0	-23.0	-25.0	-78.3	-20.6	-57.7			
Net shortwave	59.7	110.7	-51.0	21.5	84.7	-63.2	47.5	53.5	-6.0
Emissivity									
Downward longwave	235.7	244.9	-9.2	226.5	255.3	-28.8			
Upward longwave	-184.8	-188.6	3.9	-262.2	-307.8	45.6			
Net longwave	-24.9	-36.1	11.2	-35.6	-52.4	16.8	-29.5	-30.5	1.0
Sensible heat flux	-13.0	8.0	-21.0				-4.5	-7.0	2.5
Latent heat flux	11.9	14.7	-2.8				-13.5	-18.0	4.5
Ground heat flux	-3.1	-12.2	9.1						
Net surface energy	0	30.6	-54.4	-14.1	32.3	-46.4	0.0	-2.0	2.0

Table 5.7.2: Reported energy fluxes from snowpack studies.

	Ellis and Leathers 1999						Ellis and Leathers 1998		
	High albedo	Low Albedo	Difference	2.5 cm	30 cm	Difference	Snow	Snow-free	Difference
Albedo	0.80	0.50	0.30						
Downward shortwave									
Upward shortwave									
Net shortwave	56.5	129.0	-72.6				70.0	150.0	-80.0
Emissivity									
Downward longwave									
Upward longwave									
Net longwave	-42.9	-48.0	5.1	-41.8	-41.2	0.6	-60.0	-48.0	-12.0
Sensible heat flux	16.4	-7.3	23.6	40.2	45.9	5.7	30.0	-15.0	45.0
Latent heat flux	-21.8	-46.0	24.3	-5.9	-4.8	1.1	-34.0	-56.0	22.0
Ground heat flux	-2.5	-6.9	4.4	4.8	0.8	-4.1			
Net surface energy	5.7	20.8	-15.2				6.0	31.0	-25.0

REFERENCES

Baker, D. G., Ruschy, D. L., Skaggs, R. H., & Wall, D. B. (1992). Air Temperature and Radiation Depressions Associated with a Snow Cover. *Journal of Applied Meteorology*, *31*(3), 247–254. doi:10.1175/1520-0450(1992)031<0247:ATARDA>2.0.CO;2.

Chen, F., & Dudhia, J. (2001). Coupling an Advanced Land Surface–Hydrology Model with the Penn State–NCAR MM5 Modeling System. Part I: Model Implementation and Sensitivity. *Monthly Weather Review*, *129*(4), 569–585. doi:10.1175/1520-0493(2001)129<0569:CAALSH>2.0.CO;2.

Cohen, J., & Rind, D. (1991). The effect of snow cover on the climate. *Journal of Climate*, 4(7), 689-706.

Elguindi, N., Hanson, B., & Leathers, D. (2005). The Effects of Snow Cover on Midlatitude Cyclones in the Great Plains. *Journal of Hydrometeorology*, *6*(3), 263–279. doi:10.1175/JHM415.1.

Ellis, A. W., & Leathers, D. J. (1998). The effects of a discontinuous snow cover on lower atmospheric temperature and energy flux patterns. *Geophys. Res. Lett.*, *25*(12), 2161–2164. doi:10.1029/98GL01582.

Ellis, A. W., & Leathers, D. J. (1999). Analysis of Cold Airmass Temperature Modification across the U.S. Great Plains as a Consequence of Snow Depth

and Albedo. *Journal of Applied Meteorology*, *38*(6), 696–711. doi:10.1175/1520-0450(1999)038<0696:AOCATM>2.0.CO;2.

Hartmann, D. L. (1994). Global physical climatology (Vol. 56). Academic Pr.

Klingaman, N. P., Hanson, B., & Leathers, D. J. (2008). A teleconnection between forced Great Plains snow cover and European winter climate. *Journal of Climate*, 21(11), 2466-2483.

Kocin, P. J., & Uccellini, L. W. (2004). Northeast snowstorms (Vol. 32, No. 54). *Amer Meteorological Society*.

Kung, E. C., Brynson, R. A., & Lenschow, D. H. (1964). Study of a continental surface albedo on the basis of flight measurements and structure of the earth's surface cover over North America. *Monthly Weather Review*, *92*(12), 543–564. doi:10.1175/1520-0493(1964)092<0543:SOACSA>2.3.CO;2.

Leathers, D. J., Ellis, A. W., & Robinson, D. A. (1995). Characteristics of Temperature Depressions Associated with Snow Cover across the Northeast United States. *Journal of Applied Meteorology*, *34*(2), 381–390. doi:10.1175/1520-0450-34.2.381.

Mitchell, K., Duan, G. G., Moore, B., Grunmann, P., Tarpley, D., Ramsay, B., ... & Ruscher, P (2005). THE COMMUNITY Noah LAND-SURFACE MODEL (LSM) ftp://ftp.emc.ncep.noaa.gov/mmb/gcp/ldas/noahlsm/ver_2.7.1.

Namias, J. (1985). Some empirical evidence for the influence of snow cover on temperature and precipitation. *Monthly Weather Review*, 113(9), 1542-1553.

Pielke, R. A., Marland, G., Betts, R. A., Chase, T. N., Eastman, J. L., Niles, J. O.,

Niyogi, D. dutta S., et al. (2002). The influence of land-use change and landscape dynamics on the climate system: relevance to climate-change policy beyond the radiative effect of greenhouse gases. *Philosophical Transactions of the Royal Society of London. Series A: Mathematical, Physical and Engineering Sciences*, *360*(1797), 1705–1719.

Robinson, D. A., & Kukla, G. (1985). Maximum Surface Albedo of Seasonally Snow-Covered Lands in the Northern Hemisphere. *Journal of Climate and Applied Meteorology*, *24*(5), 402–411. doi:10.1175/1520-0450(1985)024<0402:MSAOSS>2.0.CO;2.

Ross, B., & Walsh, J. E. (1986). Synoptic-Scale Influences of Snow Cover and Sea Ice. *Monthly Weather Review*, *114*(10), 1795–1810. doi:10.1175/1520-0493(1986)114<1795:SSIOSC>2.0.CO;2.

Skamarock, W. C., Klemp, J. B., Dudhia, J., Gill, D. O., Barker, D. M., Duda, M. G., ... & Powers, J. G. (2008). A Description of the Advanced Research WRF Version 3.

Spar, J. (1973). Some Effects of Surface Anomalies in a Global General Circulation Model1. *Monthly Weather Review*, *101*(2), 91–100. doi:10.1175/1520-0493(1973)101<0091:SEOSAI>2.3.CO;2

Trapasso, L. M., & Simpson, R. M. (1988). The relationships between snow cover and cyclones in the Eastern United States. *The Professional Geographer*, *40*(2), 175–186. doi:10.1111/j.0033-0124.1988.00175.x.

U.S. Census Bureau. (March 2011). Population Distribution and Change: 2000 to

2010. Retrieved July, 27 2012, from http://www.census.gov/prod/cen2010/briefs/c2010br-01.pdf.

Walland, D. J., & Simmonds, I. (1996). Modelled atmospheric response to changes in Northern Hemisphere snow cover. *Climate Dynamics*, *13*(1), 25–34. doi:10.1007/s003820050150.

Walsh, J. E., & Ross, B. (1988). Sensitivity of 30-Day Dynamical Forecasts to Continental Snow cover. *Journal of Climate*, *1*(7), 739–754. doi:10.1175/1520-0442(1988)001<0739:SODDFT>2.0.CO;2

Walsh, J. E., Tucek, D. R., & Peterson, M. R. (1982). Seasonal Snow Cover and Short-Term Climatic Fluctuations over the United States. *Monthly Weather Review*, *110*(10), 1474–1486. doi:10.1175/1520-0493(1982)110<1474:SSCAST>2.0.CO;2.

Wang, W., Bruyere, C., Duda, M., Dudhia, J., Gill, D., Lin, H. C., ... & Mandel, J. (2010). ARW version 3 modeling system user's guide. Mesoscale & Miscroscale Meteorology Division. National Center for Atmospheric Research (July 2010), http://www. mmm. ucar. edu/wrf/users/docs/user_guide_V3/ARWUsersGuideV3. pdf.

Washington, W. M., & Parkinson, C. L. (2005). An introduction to three-dimensional climate modeling. Univ. Science Books. Baker, D. G., Ruschy, D. L., Skaggs, R. H., & Wall, D. B. (1992). Air Temperature and Radiation Depressions Associated with a Snow Cover. *Journal of Applied Meteorology*, *31*(3), 247–254. doi:10.1175/1520-0450(1992)031<0247:ATARDA>2.0.CO;2.

Zhang, T. (2005). Influence of the seasonal snow cover on the ground thermal regime: An overview. *Rev. Geophys.*, *43*(4), RG4002. doi:10.1029/2004RG000157.

Appendix A

LIST OF SYMBOLS

u	Eastward velocity component
v	Northward velocity component
w	Upward velocity component
μ	Atmospheric pressure difference between the top layer of the atmosphere and the surface
ϕ	Geopotential height
p	Atmospheric pressure
F	All of the body forces that arise from thermodynamic forcing, gravity, friction, and rotational effects
θ	Potential temperature
g	Gravitational acceleration
G	Soil-snow heat flux
K_{snow}	Thermal diffusivity of snow
T_{skin}	Skin temperature (kelvin)
T_{soil}	Temperature of the first layer over the physical snow depth
D_{snow}	Snow depth
α	Albedo
SW↓	Downward shortwave radiation
LW↓	Downward longwave radiation
SH	Sensible heat flux
LH	Latent heat flux
σ	Stephan-Boltmann constant
T	Temperature
ρ	Density of air
C_p	Specific heat capacity of the air
C_h	Specific heat capacity of the surface
L_v	Latent heat of vaporization
T_s	Skin temperature
T_a	Temperature of air

LE	Latent heat flux
q_s	Specific humidity of air at saturation
q_a	Specific humidity of air
S_0	Solar Constant
ε	Emissivity